



**HAL**  
open science

## Study of a low Mach nuclear core model for two-phase flows with phase transition I: stiffened gas law

Manuel Bernard, Stéphane Dellacherie, Gloria Faccanoni, Bérénice Grec,  
Yohan Penel

### ► To cite this version:

Manuel Bernard, Stéphane Dellacherie, Gloria Faccanoni, Bérénice Grec, Yohan Penel. Study of a low Mach nuclear core model for two-phase flows with phase transition I: stiffened gas law. 2012. hal-00747616v1

**HAL Id: hal-00747616**

**<https://hal.science/hal-00747616v1>**

Preprint submitted on 31 Oct 2012 (v1), last revised 29 Apr 2014 (v2)

**HAL** is a multi-disciplinary open access archive for the deposit and dissemination of scientific research documents, whether they are published or not. The documents may come from teaching and research institutions in France or abroad, or from public or private research centers.

L'archive ouverte pluridisciplinaire **HAL**, est destinée au dépôt et à la diffusion de documents scientifiques de niveau recherche, publiés ou non, émanant des établissements d'enseignement et de recherche français ou étrangers, des laboratoires publics ou privés.

# Study of a low Mach nuclear core model for two-phase flows with phase transition I: stiffened gas law

Manuel Bernard<sup>\*</sup>, Stéphane Dellacherie<sup>†</sup>,  
Gloria Faccanoni<sup>‡</sup>, Bérénice Grec<sup>§</sup> and Yohan Penel<sup>¶</sup>

October 30, 2012

In this paper, we are interested in modelling the flow of the coolant (water) in a nuclear reactor core. To this end, we use a monodimensional low Mach number model coupled to the stiffened gas law. We take into account potential phase transitions by a single equation of state which describes both pure and mixture phases. In some particular cases, we give analytical steady and/or unsteady solutions which provide qualitative information about the flow. In the second part of the paper, we introduce two variants of a numerical scheme based on the method of characteristics to simulate this model. We study and verify numerically the properties of these schemes. We finally present numerical simulations of a loss of flow accident (LOFA) induced by a coolant pump trip event.

**AMS Classifications** 35Q35, 35Q79, 65M25, 76T10.

## Introduction

Several physical phenomena have to be taken into account when modelling a water nuclear reactor such as PWRs<sup>1</sup> or BWRs<sup>2</sup> (see [8] for an introduction). In particular, the present work deals with the handling of the high thermal dilation of the coolant fluid induced by thermal transfers in nuclear cores (Figure 1 schematically pictures PWR and BWR reactors). A natural approach is to represent the evolution of the flow by means of a system of PDEs similar to the compressible

---

<sup>\*</sup>IFPEN – Lyon, BP 3, 69360 Solaize, France – manuel.bernard@ifpen.fr

<sup>†</sup>DEN/DANS/DM2S/STMF, Commissariat à l'Énergie Atomique et aux Énergies Alternatives – Saclay, 91191 Gif-sur-Yvette, France – stephane.dellacherie@cea.fr

<sup>‡</sup>Université du Sud Toulon-Var – IMATH, EA 2134, avenue de l'Université, 83957 La Garde, France – faccanon@univ-tln.fr

<sup>§</sup>MAP5 UMR CNRS 8145 - Université Paris Descartes - Sorbonne Paris Cité, 45 rue des Saints Pères, 75270 Paris Cedex 6, France – berenice.grec@parisdescartes.fr

<sup>¶</sup>CETMEF-INRIA – team ANGE and LJLL UMR CNRS 7598, 4 place Jussieu, 75005 Paris, France – yohan.penel@gmail.com

<sup>1</sup>PWR is the acronym for Pressurized Water Reactor.

<sup>2</sup>BWR is the acronym for Boiling Water Reactor.

Navier-Stokes equations coupled to the modelling of phase transition which is the case in classical industrial codes [1, 4, 20].

In nominal and incidental situations as well as in some accidental situations studied in safety evaluations, the magnitude of the sound velocity is much higher than the one of the velocity of the coolant fluid, which means that the Mach number of the flow is small. The discretization of compressible Navier-Stokes type systems may induce numerical issues directly related to the existence of fast acoustic waves even in low Mach number flows (see for example [11, 15, 16, 22] when the convective part of the compressible Navier-Stokes system is discretized by means of a Godunov type scheme).

Nevertheless, in a low Mach number regime, the acoustic phenomena can be neglected in energy balances although the flow is highly compressible because of the thermal dilation. Thus, to overcome the numerical difficulties, S. Dellacherie proposed in [12] another model obtained by filtering out the acoustic waves in the compressible model. Let us underline that this approach was applied to model firstly low Mach combustion phenomena [26] and then thermal dilation of the interface of bubbles at low Mach number [9, 10, 28]. The low Mach number model derived in [12] and called the *Low Mach Nuclear Core (LMNC) model* was discretized in [3] in the monodimensional (1D) case. Moreover, 1D unsteady analytical solutions were also given in [3] which allowed to validate the numerical schemes.

Despite relevant numerical results, the approach proposed in [3, 12] was not satisfying since in particular, it was restricted to monophasic flows. Thus, we extend in this study the results stated in [3, 12] by taking into account phase transition in the LMNC model. If we neglect diffusion terms, the LMNC model proposed in this paper may be seen as the low Mach number limit of the Homogeneous Equilibrium Model (HEM) [7] with source terms. Let us recall that the HEM model is the compressible Euler system in which the two phases are supposed to be at local kinematic and thermodynamical equilibria.

A crucial step in the process is the modelling of properties of the fluid through the equation of state. It is important from a physical point of view to match experimental data and from a mathematical point of view to close the system of PDEs. In the present work, this point is achieved by using the stiffened gas law. A major result in this paper is the exhibition of 1D unsteady analytical solutions with phase transition (see Proposition 6). These solutions are of great importance: on the one hand to accurately estimate heat transfers in a nuclear core in incidental and accidental situations, and on the other hand to assess the robustness of the monodimensional numerical schemes presented in this article.

At last, we wish to underline that although this study is specific to dimension 1 (which is essential to obtain in particular the unsteady analytical solutions with phase change), it remains useful from an industrial point of view since many safety evaluations use a 1D modelling to describe the flow in each component of the nuclear reactor and, thus, in the nuclear core. Nevertheless, the extension of this work to the 2D and 3D cases is a natural and important perspective.

This paper is organized as follows. In the first section, the LMNC model is recalled under some assumptions, and we study the existence of (more or less) equivalent formulations of the model that can be used depending on the variables we aim at focusing on. The second section is devoted to the modelling of phase transition and to the EOS that is needed to close the system. In the third section, we prove some theoretical results stated (but not proved) in [3] and we extend them

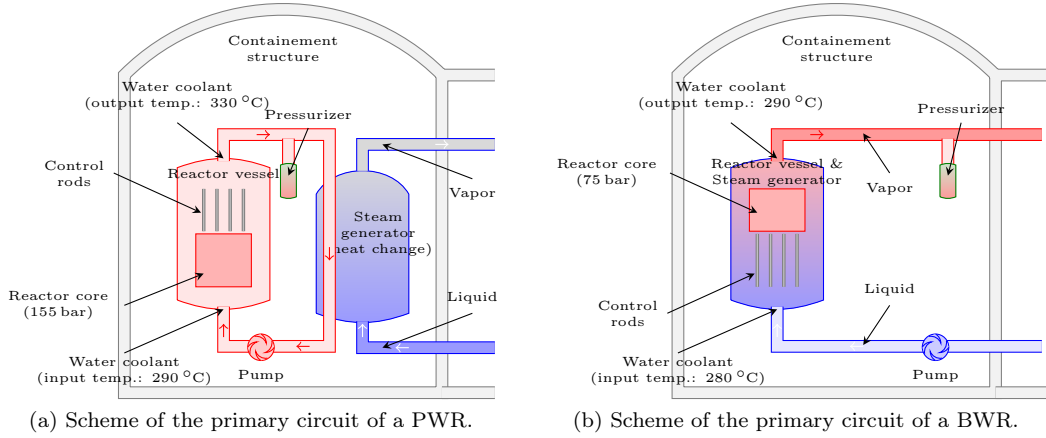


Figure 1: Scheme of nuclear reactors whose coolant is water: the major difference between PWR and BWR is the steam void formation in the core of the latter.

to the multiphasic case. Exact and asymptotic solutions are thus exhibited. Numerical aspects are then investigated in the fourth section where a new version of the method of characteristics is presented. This scheme is then applied in the fifth section to various situations with occurrence of phase transition.

## 1 The low Mach nuclear core model

The Low Mach Nuclear Core (LMNC) model introduced in [12] is obtained by filtering out the acoustic waves in a compressible Navier-Stokes type system. This is achieved through an asymptotic expansion with respect to the Mach number assumed to be very small in this framework. One of the major consequences is the modification of the nature of the equations: the filtering out of the acoustic waves – which are solutions of a hyperbolic equation in the compressible system – introduces a new unknown (namely the dynamic pressure) which is solution to an elliptic equation in the LMNC model. Another consequence is that we are able to compute explicit monodimensional unsteady solutions of the LMNC model with or without phase transition<sup>3</sup> (see section 3) and to construct 1D robust and accurate numerical schemes<sup>4</sup> (see section 4).

In this section, we recall the LMNC model and we present equivalent formulations for smooth solutions. Since we are interested in the 1D case in this paper, we do not extend results to 2D/3D. Nevertheless, this can easily be done (provided the boundary conditions are adapted).

<sup>3</sup>This is not the case for the 1D compressible system from which the LMNC is derived.

<sup>4</sup>The existence of fast acoustic waves in the compressible system induces numerical difficulties – see [11,22] for example – which cannot arise in the LMNC model since the acoustic waves have been filtered out to obtain this low Mach number model.

## 1.1 Governing equations

The 1D nonconservative formulation of the LMNC model [12] is written as

$$\begin{cases} \partial_y v = \frac{\beta(h, p_0)}{p_0} \Phi(t, y), & (1a) \\ \rho(\partial_t h + v \partial_y h) = \Phi(t, y), & (t, y) \in \mathbb{R}^+ \times [0, L] & (1b) \\ \partial_t(\rho v) + \partial_y(\rho v^2 + \bar{p}) = F(v) - \rho g, & (1c) \end{cases}$$

where  $v$  and  $h$  denote respectively the velocity and the enthalpy of the fluid. The density  $\rho = \rho(h, p = p_0)$  is related to the enthalpy by an equation of state (EOS – see section 2). So does the dimensionless compressibility coefficient  $\beta(h, p_0)$  which is defined by

$$\beta(h, p_0) \stackrel{\text{def}}{=} -\frac{p_0}{\rho^2(h, p_0)} \cdot \frac{\partial \rho}{\partial h}(h, p_0). \quad (2)$$

The power density  $\Phi(t, y)$  is a given function of time and space modelling the heating of the coolant fluid due to the fission reactions in the nuclear core. Finally,  $g$  is the gravity field and  $F(v)$  models viscous effects: the classical internal friction in the fluid, and also the friction on the fluid due to technological devices in the nuclear core (*e.g.* the friction on the fluid due to the fuel rods). In the sequel, we take

$$F(v) = \partial_y(\mu \partial_y v).$$

In this case,  $\mu$  is a turbulent viscosity given by an homogenized turbulent model. Nevertheless, we explain in the sequel that the exact choice of  $F(v)$  is not important in the 1D case (this is no more the case in 2D/3D).

We must also emphasize that model (1) is characterized by two pressure fields, which is classical in low Mach number approaches: the *thermodynamic pressure*  $p_0$  is involved in the equation of state and the *dynamic pressure*  $\bar{p}$  appears in equation (1c). In the 1D case, equation (1c) decouples from the two other equations and may be considered as a post-processing leading to the computation of  $\bar{p}$  (this is why the expression of  $F(v)$  is not really important in 1D). Thus, equation (1c) will often be left apart in the sequel and equations (1a)-(1b) will often be referred to as the LMNC model for the sake of simplicity.

From now on, we suppose that:

### Hypothesis 1.

1.  $\Phi(t, y) \geq 0$  for all  $(t, y) \in \mathbb{R}^+ \times [0, L]$ ;
2.  $p_0$  is a positive constant.

The first assumption characterizes the fact that we study a nuclear core where the coolant fluid is heated. In the steam generator of a PWR type reactor (see Figure 1(a)) – which could also be modelled with a LMNC type model, we would have  $\Phi(t, y) \leq 0$ . The second assumption is justified by the fact that a negative thermodynamic pressure does not have any physical sense in our context.

**Boundary conditions** The fluid is injected at the bottom of the core at a given enthalpy  $h_e$  and at a given flow rate  $D_e$ . We also impose the dynamic pressure  $\bar{p}$  at the exit of the core ( $y = L$ ). The boundary conditions are thus written as

$$h(t, 0) = h_e(t), \quad (\rho v)(t, 0) = D_e(t), \quad \bar{p}(t, L) = p_0.$$

The entrance velocity  $v_e(t)$  to apply at  $y = 0$  is deduced from the relation  $v_e(t) = D_e(t)/\rho_e(t)$  where  $\rho_e = \rho(h_e, p = p_0)$ . The fact that  $h_e$  and  $D_e$  depend on time enables to model transient regimes induced by accidental situations. For example, when  $D_e(t)$  tends to zero, it models a main coolant pump trip event which is a *Loss Of Flow Accident* (LOFA) as at the beginning of the Fukushima accident in the reactors 1, 2 and 3.

We also assume in the sequel that:

**Hypothesis 2.**

1.  $D_e$  is non-negative.
2.  $h_e$  is such that  $\rho_e$  is well-defined and positive.

The first assumption corresponds to a nuclear power plant of PWR or BWR type: the flow is *upward*<sup>5</sup>. The second assumption means that the EOS  $\rho(h, p)$  is such that  $\rho(h_e, p_0)$  can be computed. Moreover, we also suppose that  $\rho(h_e, p_0) > 0$  since a negative density does not have any physical sense in our context.

We finally make the following modelling hypothesis:

**Hypothesis 3.**  $\beta$  is non-negative.

Positivity assumptions about  $\Phi$ ,  $D_e$ ,  $\beta$  and  $\rho$  in Hypotheses 1, 2 and 3 ensure that the velocity  $v(t, y)$  remains non-negative at any time and anywhere in the core. Otherwise, the system could become ill-posed (see section 4.2 in [12] where this question is partially studied).

**Well-prepared initial conditions** The model is finally closed by means of initial conditions  $h(0, y) = h_0(y)$  and  $(\rho v)(0, y) = D_0(y)$ . However, these data cannot be randomly chosen. Indeed, as system (1) consists of steady and unsteady equations, the initial velocity  $v_0$  must satisfy equation (1a) for  $t = 0$ , which means

$$v_0'(y) = \frac{\beta(h_0(y), p_0)}{p_0} \Phi(0, y).$$

Hence,  $h_0$  prescribes both the initial density through the EOS and the initial velocity through the previous equality (together with the compatibility condition  $v_0(0) = v_e(0)$ ). We then deduce  $D_0 = \rho_0 v_0$ . When this condition holds, such initial data  $(h_0, D_0)$  are said to be *well-prepared*. This will be implicitly assumed in the sequel.

---

<sup>5</sup> The flow could be downward when the nuclear reactor is a material testing reactor.

## 1.2 Origin and different formulations of the model

The 1D LMNC model (1) is written in [12] as

$$\begin{cases} \partial_y v = \frac{\beta(h, p_0)}{p_0} \Phi(t, y), \\ \rho(h, p_0) \cdot (\partial_t h + v \partial_y h) = \Phi(t, y). \end{cases} \quad \begin{matrix} (3a) \\ (3b) \end{matrix}$$

We recall that in the 1D case, equation (1c) is a post-processing of (3). It is important to note that the low Mach number model (3) is justified only under smoothness assumptions. To study the existence of weak solutions, it might be better to use a conservative formulation which is equivalent to (3) for smooth solutions. This conservative formulation is the following:

**Proposition 1.** *Under smoothness assumptions, system (3) is equivalent to*

$$\begin{cases} \partial_t \rho + \partial_y(\rho v) = 0, \\ \partial_t(\rho h) + \partial_y(\rho h v) = \Phi(t, y). \end{cases} \quad \begin{matrix} (4a) \\ (4b) \end{matrix}$$

System (4) (coupled to equation (1c)) is the LMNC model written in conservative variables. Although (4) is more general than (3), system (3) is interesting as it stresses on the fact that the filtering out of the acoustic waves turns the hyperbolic nature of the compressible Navier-Stokes system (related to the acoustic waves) to an elliptic constraint similar to the incompressible case.

*Proof of Proposition 1.*

- $\Rightarrow$  According to definition (2) of  $\beta$ , we have

$$\partial_t \rho + \partial_y(\rho v) = \frac{\partial \rho}{\partial h} \underbrace{(\partial_t h + v \partial_y h)}_{\stackrel{(3b)}{=} \frac{\Phi}{\rho}} + \underbrace{\rho \partial_y v}_{\stackrel{(3a)}{=} \frac{\beta \Phi}{p_0}} = 0 \quad (5)$$

which gives (4a). We also obtain

$$\partial_t(\rho h) + \partial_y(\rho h v) = h(\partial_t \rho + \partial_y(\rho v)) + \rho(\partial_t h + v \partial_y h) = \Phi.$$

Using (3b) and (4a), we recover (4b).

- $\Leftarrow$  Because of (4a), we deduce (3b) from (4b). Moreover, we deduce from (4a) and (3b) that

$$\partial_t \rho + \partial_y(\rho v) = \frac{\partial \rho}{\partial h} (\partial_t h + v \partial_y h) + \rho \partial_y v = \frac{\partial \rho}{\partial h} \cdot \frac{\Phi}{\rho} + \rho \partial_y v = 0,$$

which gives (3a) thanks to definition (2) of  $\beta$ . □

Moreover, under smoothness assumptions and for a particular class of EOS, we can derive a semi-conservative formulation equivalent to (3), and which may be useful to derive efficient numerical schemes. Indeed, we have the following proposition.

**Proposition 2.** *Under smoothness assumptions:*

1. System (3) implies

$$\begin{cases} \partial_y v = \frac{\beta(h, p_0)}{p_0} \Phi(t, y), \\ \partial_t(\rho(h, p_0)h) + \partial_y(\rho(h, p_0)hv) = \Phi(t, y). \end{cases} \quad (6a)$$

2. For equations of state such that

$$\frac{\partial \rho}{\partial h}(h, p_0) \neq -\frac{\rho(h, p_0)}{h}, \quad (7)$$

systems (3) and (6) are equivalent.

This new formulation will be a perspective of great interest for the extension to dimension 2, especially in view of the method developed in [5]. Nevertheless, condition (7) upon  $\rho$  seems to be quite restrictive insofar as it does not enable to handle perfect gas (for which  $\frac{\partial \rho}{\partial h} = -\frac{\rho}{h}$ ). In the latter case, equations (6a) and (6b) are nothing but the same equation, which implies that we have to use formulations (3) or (4).

*Proof of Proposition 2.* The first point is a direct consequence of Proposition 1 since

$$\partial_t(\rho(h, p_0)h) + \partial_y(\rho(h, p_0)hv) = \underbrace{\rho(h, p_0) \cdot (\partial_t h + v \partial_y h)}_{\stackrel{(3b)}{=} \Phi} + h \underbrace{[\partial_t(\rho(h, p_0)) + \partial_y(\rho(h, p_0)v)]}_{\stackrel{(5)}{=} 0}.$$

To prove the second point, we just have to show that (6) implies (3) under condition (7). On the one hand, since

$$\partial_t \rho + \partial_y(\rho v) = \frac{\partial \rho}{\partial h}(h, p_0)(\partial_t h + v \partial_y h) + \rho(h, p_0) \partial_y v,$$

by using (2) and (6a), we obtain

$$\partial_t \rho + \partial_y(\rho v) = \frac{\partial \rho}{\partial h}(h, p_0) \left( \partial_t h + v \partial_y h - \frac{\Phi}{\rho(h, p_0)} \right). \quad (8)$$

On the other hand, (6b) leads to

$$\rho(h, p_0) \cdot (\partial_t h + v \partial_y h) + h [\partial_t(\rho(h, p_0)) + \partial_y(\rho(h, p_0)v)] = \Phi(t, y)$$

that is to say

$$\partial_t \rho + \partial_y(\rho v) = -\frac{\rho(h, p_0)}{h} \left( \partial_t h + v \partial_y h - \frac{\Phi}{\rho(h, p_0)} \right). \quad (9)$$

Thus, by comparing (8) and (9), we obtain

$$\partial_t h + v \partial_y h - \frac{\Phi}{\rho(h, p_0)} = 0$$

under condition (7), which proves that (6) implies (3).  $\square$

**Remark 1.** *The equivalence between systems (3), (4) and (6) also holds in higher dimensions. Nevertheless, the momentum equation is strongly coupled to the other equations in 2D/3D and must be taken into account under conservative or under nonconservative form. Indeed, these forms are equivalent as soon as the unknowns are smooth and the mass conservation law holds.*

**Remark 2.** *A generalization of this model would consist in taking into account the thermal conductivity. In this case, it is convenient to work with another formulation of the model where the temperature is considered as the main variable instead of the enthalpy. The equation of state then becomes  $\rho = \rho(T, p = p_0)$ . However, this equation of state is no longer invertible when phase transition occurs (see section 2 for more details).*

## 2 Equation of state for two-phase fluids

For the system to be closed, an additional equation is required: the equation of state (EOS). It corresponds to the modelling of thermodynamical properties and consists of an algebraic relation between thermodynamical variables. The issue is here to construct an EOS that models all phases of a fluid. Indeed, perturbations of the inlet velocity or of the power density may strongly modify the temperature in the fluid and cause phase transition from liquid phase to vapor phase. At this modelling scale, the fluid can thus be under liquid, vapor or mixture phases.

The model used in this study is based on the assumption of local kinematic and thermodynamical equilibria between phases. This means that the phases are assumed to move at the same velocity, that vaporisation, condensation and heat transfer processes are assumed to be instantaneous. As a consequence, the two-phase flow can be considered as a single-phase problem provided the EOS  $(h, p) \mapsto \rho(h, p)$  (and thus the compressibility coefficient  $\beta$  defined by (2)) takes phase transition into account. With this modelling, the two-phase flow evolution at low Mach number can be described by means of the LMNC model (1). In this case and when viscous effects modelled by  $F(v)$  in (1c) are neglected, the LMNC model (1) is the low Mach limit of the Homogeneous Equilibrium Model (HEM) [7] with source terms.

### 2.1 General thermodynamics

In classical thermodynamics, two variables are sufficient to represent a thermodynamical state of a pure single-phase fluid. This is done by means of an EOS which is a relation between the internal energy, the density and the entropy. In the literature, there exist numerous EOS specific to the fluid and to the model which are considered. In the case of liquid-vapor phase transitions, the EOS must not only represent the behavior of each pure phase (liquid or vapor), but also model the evolution of a mixture. Its behavior is coarsely pictured on Figure 2a.

There may be a mixture region where the two phases coexist: it is called the *saturation zone*. This region is bounded by two curves connected at the critical point  $(1/\rho_c, p_c)$  which also belongs to the critical isotherm  $T = T_c$ . Another curve of interest is the coexistence curve  $p^s(T)$  which relates the pressure to the temperature at saturation (see Figure 2b).

These curves can be obtained experimentally (see [25] for instance) and correspond to thermodynamical equilibria of temperature, pressure and Gibbs potential of the two phases. The Van der Waals law associated to the Maxwell construction is the most common example of this kind of EOS.

Nevertheless, it is very complicated to derive a unique EOS describing accurately both pure and mixture phases. To better handle pure phases and saturation curves, an idea consists in using two laws (one for each phase) so that each phase has its own thermodynamics. In the following section we detail the general construction of the EOS in the mixture region given one EOS for each phase.

### 2.2 Construction of the EOS in the mixture

The difficulty using this approach is to specify a unique EOS that can model all possible states for the fluid: pure liquid, pure vapor and two-phase mixture. In this section, we explain how to specify the EOS in the mixture given an EOS for each pure phase. We then adapt these results when pure phases are governed by the *stiffened gas law*.

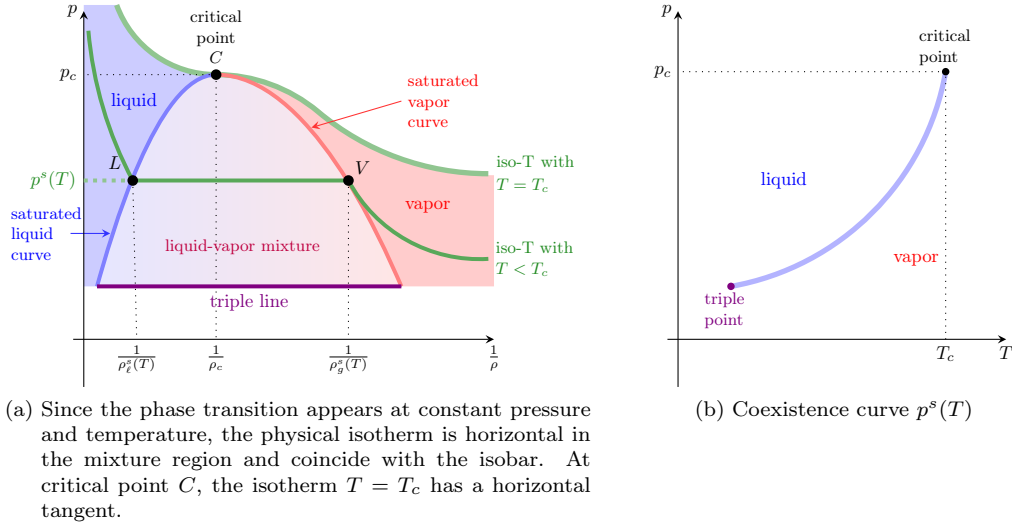


Figure 2: Saturation and coexistence curves.

**Characterization of the two-phase media** We consider each phase  $\kappa$  as a compressible fluid governed by a given EOS that is a function  $(\rho, \varepsilon) \mapsto \eta_\kappa$  where  $\rho$ ,  $\varepsilon$  and  $\eta_\kappa$  denote respectively the specific density, the specific internal energy and the specific entropy of the fluid. We assume that  $\eta_\kappa$  has a *negative-definite Hessian matrix*.

We then define classically for phase  $\kappa = \ell$  (liquid phase) and phase  $\kappa = g$  (vapor phase) the temperature  $T_\kappa \stackrel{\text{def}}{=} 1/[(\partial\eta_\kappa/\partial\varepsilon)_\rho]$ , the pressure  $p_\kappa \stackrel{\text{def}}{=} -\rho^2 T_\kappa (\partial\eta_\kappa/\partial\rho)_\varepsilon$  and the chemical potential  $g_\kappa \stackrel{\text{def}}{=} \varepsilon + p_\kappa/\rho - T_\kappa \eta_\kappa$ . Finally  $\alpha$  denotes the volume fraction of vapor phase. This variable characterizes the volume of vapor in each unit volume:  $\alpha = 1$  means that this volume is completely filled by vapor; similarly, a full liquid volume corresponds to  $\alpha = 0$ . Liquid and vapor are thus characterized by their thermodynamical properties.

The mixture density  $\rho$  and the mixture internal energy  $\varepsilon$  are defined by

$$\begin{cases} \rho = \alpha\rho_g + (1 - \alpha)\rho_\ell, & (10a) \\ \rho\varepsilon = \alpha\rho_g\varepsilon_g + (1 - \alpha)\rho_\ell\varepsilon_\ell, & (10b) \end{cases}$$

where  $\rho_g$ ,  $\rho_\ell$ ,  $\varepsilon_g$  and  $\varepsilon_\ell$  denote respectively vapor/liquid densities and vapor/liquid internal energies. Recalling that the internal energy is connected to the enthalpy by the relation  $\rho h = \rho\varepsilon + p$ , we can compute the mixture enthalpy  $h$  when the pressure is the same in both phases (which is the case in the LMNC model where the thermodynamical pressure  $p$  is constant and equal to  $p_0$ ). This leads to

$$\rho h = \alpha\rho_g h_g + (1 - \alpha)\rho_\ell h_\ell, \quad (11)$$

where  $h_g$ ,  $h_\ell$  are respectively vapor/liquid enthalpies.

When taking phase transition into account, the two-phase mixture is constructed according to the second principle of thermodynamics. The key idea is that, when phases coexist (*i.e.* when  $0 < \alpha < 1$ ), they have the same pressure, the same temperature and their chemical potentials

are equal. The corresponding temperature, noted  $T^s$  for *temperature at saturation*, is obtained by expliciting the equality of chemical potentials  $g_\ell(p, T^s) = g_g(p, T^s)$ . This implies a relation between  $T^s$  and  $p$  (see for example [6, 18, 21] for more details). In the sequel we choose to express the temperature in the mixture as a function of the pressure and we define functions at saturation  $\rho_\kappa^s$  and  $h_\kappa^s$  by  $p \mapsto \rho_\kappa^s \stackrel{\text{def}}{=} \rho_\kappa(p, T^s(p))$  and  $p \mapsto h_\kappa^s \stackrel{\text{def}}{=} h_\kappa(p, T^s(p))$ . Consequently, all thermodynamical quantities can be expressed as functions of the enthalpy and the pressure as it will be seen below. The choice to focus on pressure relies on the fact that the pressure in the LMNC model is supposed to be constant and equal to  $p_0$ . Notice that for most fluids  $h_\ell^s < h_g^s$  (see [25]).

**Density of the two-phase media** Given functions at saturation, we are now able to model density in pure and mixture phases. Using equations (10a) and (11), the density is written as a function of enthalpy  $h$  and pressure  $p$  as follows

$$\rho(h, p) = \begin{cases} \rho_\ell(h, p), & \text{if } h \leq h_\ell^s(p), \\ \rho_m(h, p) \stackrel{\text{def}}{=} \frac{[\rho_g^s \rho_\ell^s (h_g^s - h_\ell^s)](p)}{[\rho_g^s h_g^s - \rho_\ell^s h_\ell^s](p) - h \cdot [\rho_g^s - \rho_\ell^s](p)}, & \text{if } h_\ell^s(p) < h < h_g^s(p), \\ \rho_g(h, p), & \text{if } h \geq h_g^s(p). \end{cases} \quad (12)$$

**Temperature of the two-phase media** The temperature in the mixture  $T^s$  is implicitly defined by the equation  $g_\ell(p, T^s) = g_g(p, T^s)$  so that the temperature depends continuously on the enthalpy and on the pressure and reads

$$T(h, p) = \begin{cases} T_\ell(h, p), & \text{if } h \leq h_\ell^s(p), \\ T^s(p), & \text{if } h_\ell^s(p) < h < h_g^s(p), \\ T_g(h, p), & \text{if } h \geq h_g^s(p). \end{cases} \quad (13)$$

We must emphasize that the function  $h \mapsto T(h, p = p_0)$  cannot be inverted in the mixture zone for a constant pressure (as it is the case in the LMNC model). This remark prevents from working with equations on  $T$  instead of equations on  $h$  (see Remark 2).

**Compressibility coefficient of two-phase media** Computing the derivative of the density (12), we obtain the compressibility coefficient  $\beta$  (previously defined by (2))

$$\beta(h, p) \stackrel{\text{def}}{=} -\frac{p}{\rho^2} \cdot \frac{\partial \rho}{\partial h} \Big|_p = \begin{cases} \beta_\ell(h, p), & \text{if } h \leq h_\ell^s(p), \\ \beta_m(p) \stackrel{\text{def}}{=} -p \cdot \left[ \frac{\rho_g^s - \rho_\ell^s}{\rho_g^s \rho_\ell^s (h_g^s - h_\ell^s)} \right](p), & \text{if } h_\ell^s(p) < h < h_g^s(p), \\ \beta_g(h, p), & \text{if } h \geq h_g^s(p). \end{cases} \quad (14)$$

We notice that independently of the EOS in the pure phases, the compressibility coefficient is constant in the mixture (since the pressure is constant in the LMNC model). Moreover, it is generally discontinuous between pure and mixture phases.

**Speed of sound of two-phase media** In [2, 18, 19] it has been proven that the speed of sound is always positive when using the previous approach. To compute explicitly the speed of sound as a function of the enthalpy and the pressure, we start from the usual thermodynamical relation

$$T d\eta = d\varepsilon - \frac{p}{\rho^2} d\rho.$$

On the one hand, the relation  $h = \varepsilon + \frac{p}{\rho}$  coupled to the previous statement leads to

$$d(\rho\varepsilon) = (\rho T)d\eta + hd\rho.$$

On the other hand, we have

$$d(\rho\varepsilon) = \left. \frac{\partial(\rho\varepsilon)}{\partial\rho} \right|_p d\rho + \left. \frac{\partial(\rho\varepsilon)}{\partial p} \right|_\rho dp.$$

Therefore, the comparison of the two previous equalities yields

$$dp = \frac{h - \left. \frac{\partial(\rho\varepsilon)}{\partial\rho} \right|_p}{\left. \frac{\partial(\rho\varepsilon)}{\partial p} \right|_\rho} d\rho + \frac{\rho T}{\left. \frac{\partial(\rho\varepsilon)}{\partial p} \right|_\rho} d\eta,$$

so that the speed of sound  $c^*$  is given by

$$(c^*)^2 \stackrel{\text{def}}{=} \left. \frac{\partial p}{\partial\rho} \right|_\eta = \frac{h - \left. \frac{\partial(\rho\varepsilon)}{\partial\rho} \right|_p}{\left. \frac{\partial(\rho\varepsilon)}{\partial p} \right|_\rho} = \frac{h - \left. \frac{\partial(\rho h)}{\partial\rho} \right|_p}{\left. \frac{\partial(\rho h)}{\partial p} \right|_\rho - 1}, \quad (15)$$

since  $\rho\varepsilon = \rho h - p$ .

- In the pure phase  $\kappa$ , the volume fraction  $\alpha$  is 0 or 1, so that  $\rho = \rho_\kappa$ ,  $h = h_\kappa$  and equation (15) becomes

$$(c_\kappa^*)^2 = \frac{-\rho_\kappa \left. \frac{\partial h_\kappa}{\partial\rho_\kappa} \right|_p}{\rho_\kappa \left. \frac{\partial h_\kappa}{\partial p} \right|_{\rho_\kappa} - 1}. \quad (16a)$$

- In the mixture, using (11) and noticing that  $\rho_\kappa h_\kappa = \rho_\kappa^s h_\kappa^s$  (since  $T = T^s(p)$  in the mixture), which only depends on  $p$ , we can write

$$\begin{aligned} \left. \frac{\partial(\rho h)}{\partial\rho} \right|_p &= \left. \frac{\partial\alpha}{\partial\rho} \right|_p (\rho_g^s h_g^s) + \alpha \left. \frac{\partial(\rho_g^s h_g^s)}{\partial\rho} \right|_p - \left. \frac{\partial\alpha}{\partial\rho} \right|_p (\rho_\ell^s h_\ell^s) + (1-\alpha) \left. \frac{\partial(\rho_\ell^s h_\ell^s)}{\partial\rho} \right|_p, \\ \left. \frac{\partial(\rho h)}{\partial p} \right|_\rho &= \left. \frac{\partial\alpha}{\partial p} \right|_\rho (\rho_g^s h_g^s) + \alpha \left. \frac{\partial(\rho_g^s h_g^s)}{\partial p} \right|_\rho - \left. \frac{\partial\alpha}{\partial p} \right|_\rho (\rho_\ell^s h_\ell^s) + (1-\alpha) \left. \frac{\partial(\rho_\ell^s h_\ell^s)}{\partial p} \right|_\rho. \end{aligned}$$

Because of (10a), we compute the partial derivatives of the volume fraction  $\alpha$

$$\begin{aligned} \left. \frac{\partial\alpha}{\partial\rho} \right|_p &= \frac{1}{\rho_g^s - \rho_\ell^s}, \\ \left. \frac{\partial\alpha}{\partial p} \right|_\rho &= \frac{-(\rho_\ell^s)'(\rho_g^s - \rho_\ell^s) - (\rho - \rho_\ell^s)((\rho_g^s)' - (\rho_\ell^s)')}{(\rho_g^s - \rho_\ell^s)^2} = -\frac{\alpha(\rho_g^s)' + (1-\alpha)(\rho_\ell^s)'}{\rho_g^s - \rho_\ell^s}, \end{aligned}$$

where  $(\rho_\kappa^s)'$  is the derivative of  $p \mapsto \rho_\kappa^s(p)$ . Hence:

$$(c_m^*(h, p))^2 \stackrel{\text{def}}{=} \frac{h - \frac{\rho_g^s h_g^s - \rho_\ell^s h_\ell^s}{\rho_g^s - \rho_\ell^s}}{-(\alpha(\rho_g^s)' + (1-\alpha)(\rho_\ell^s)') \frac{\rho_g^s h_g^s - \rho_\ell^s h_\ell^s}{\rho_g^s - \rho_\ell^s} + \alpha(\rho_g^s h_g^s)' + (1-\alpha)(\rho_\ell^s h_\ell^s)' - 1}. \quad (16b)$$

Finally, the speed of sound is given by

$$c^*(h, p) = \begin{cases} c_\ell^*(h, p), & \text{if } h \leq h_\ell^s(p), \\ c_m^*(h, p), & \text{if } h_\ell^s(p) < h < h_g^s(p), \\ c_g^*(h, p), & \text{if } h \geq h_g^s(p). \end{cases} \quad (17)$$

**Remark 3.** *The speed of sound is discontinuous across the saturation curve, and it is smaller in the mixture than in any pure phase. The minimum value is reached for void ratios close to zero (see [18]).*

### 2.3 The stiffened gas EOS

Several EOS can be considered to describe thermodynamical properties of pure phases. In this paper (like in [3]) we use the *stiffened gas law*. This EOS is the simplest prototype that contains the main physical properties of pure fluids such as repulsive and attractive molecular effects, thereby facilitating the handling of thermodynamics through a simple analytical formulation. It is a generalization of the well-known *ideal gas law* (which is a commonly used EOS to describe the vapor phase), and it is an acceptable model for the liquid phase (for more details see the appendix).

The complete form of the stiffened gas EOS is written as

$$(\rho, \varepsilon) \mapsto \eta = c_v \ln(\varepsilon - q - \pi/\rho) - c_v(\gamma - 1) \ln \rho + m, \quad (18)$$

where  $\eta$  is the entropy written as a function of the density  $\rho$  and the internal energy  $\varepsilon$ . The parameters  $c_v > 0$  (specific heat at constant volume),  $\gamma > 1$  (adiabatic coefficient),  $\pi$  (constant reference pressure),  $q$  (binding energy) and  $m$  (reference entropy) are some constants describing thermodynamical properties of the phase. Note that the case of an ideal gas EOS is recovered by setting  $\pi$  and  $q$  to zero. For  $\eta$  to be well-defined, it is necessary to have  $\rho > 0$  and  $\varepsilon - q - \pi/\rho > 0$ .

The term  $(\gamma - 1)(\varepsilon - q)\rho > 0$  models repulsive effects that are present for any state (gas, liquid or solid) and is due to molecular vibrations. The constant  $\gamma\pi > 0$  represents the attractive molecular effect that guarantees the cohesion of matter in liquid or solid phases (hence  $\pi = 0$  for gas).

The classical definitions in thermodynamics provide the following expressions for the temperature  $T$ , the pressure  $p$ , the enthalpy  $h$  and the Gibbs potential  $g$  as functions of the density  $\rho$  and the internal energy  $\varepsilon$ :

$$\begin{aligned} p(\rho, \varepsilon) &\stackrel{\text{def}}{=} -T\rho^2 \left. \frac{\partial \eta}{\partial \rho} \right|_\varepsilon = (\gamma - 1)(\varepsilon - q - \pi/\rho)\rho - \pi = (\gamma - 1)(\varepsilon - q)\rho - \gamma\pi, \\ T(\rho, \varepsilon) &\stackrel{\text{def}}{=} \left( \left. \frac{\partial \eta}{\partial \varepsilon} \right|_\rho \right)^{-1} = \frac{\varepsilon - q - \pi/\rho}{c_v}, \\ h(\rho, \varepsilon) &\stackrel{\text{def}}{=} \varepsilon + \frac{p}{\rho} = q + (\varepsilon - q - \pi/\rho)\gamma, \\ g(\rho, \varepsilon) &\stackrel{\text{def}}{=} \varepsilon - T\eta + \frac{p}{\rho} = q + (\varepsilon - q - \pi/\rho) \left( \gamma - \frac{m}{c_v} - \ln((\varepsilon - q - \pi/\rho)\rho^{1-\gamma}) \right). \end{aligned}$$

**Remark 4.** *Since we assumed  $\varepsilon - q - \pi/\rho > 0$  and  $\gamma > 1$ , the definition of the enthalpy implies that  $h - q > 0$ .*

**Temperature and enthalpy at saturation** We assume that each phase  $\kappa$  is described by its own stiffened gas EOS. To complete the results from section 2.2, we have to express the temperature at saturation. As the temperature is constant in the mixture, we make a change of thermodynamical variables from  $(\rho, \varepsilon)$  to  $(p, T)$  which can be made explicit for this kind of EOS. The variables are now given by

$$\begin{aligned}\rho_\kappa(p, T) &= \frac{p + \pi_\kappa}{(\gamma_\kappa - 1)c_{v_\kappa} T}, \\ \varepsilon_\kappa(p, T) &= c_{v_\kappa} T \frac{p + \pi_\kappa \gamma_\kappa}{p + \pi_\kappa} + q_\kappa, \\ h_\kappa(p, T) &= q_\kappa + \gamma_\kappa c_{v_\kappa} T, \\ g_\kappa(p, T) &= q_\kappa + T \left( c_{v_\kappa} \gamma_\kappa - q'_\kappa - c_{v_\kappa} \gamma_\kappa \ln T + c_{v_\kappa} (\gamma_\kappa - 1) \ln(p + \pi_\kappa) \right),\end{aligned}$$

where for the sake of simplicity we denoted  $q'_\kappa \stackrel{\text{def}}{=} m_\kappa + c_{v_\kappa} \gamma_\kappa \ln c_{v_\kappa} + c_{v_\kappa} (\gamma_\kappa - 1) \ln(\gamma_\kappa - 1)$  as in [23, 30]. We are now able to define the temperature at saturation  $T^s$  as the solution of the equation  $g_\ell(p, T^s) = g_g(p, T^s)$  which yields

$$(c_{v_g} \gamma_g - c_{v_\ell} \gamma_\ell) (1 - \ln T^s(p)) - (q'_g - q'_\ell) + c_{v_g} (\gamma_g - 1) \ln(p + \pi_g) - c_{v_\ell} (\gamma_\ell - 1) \ln(p + \pi_\ell) = \frac{q_\ell - q_g}{T^s(p)}.$$

We remark that if  $q_\ell = q_g$  or if  $c_{v_g} \gamma_g = c_{v_\ell} \gamma_\ell$ , we can compute  $T^s$  analytically. Otherwise, a Newton algorithm can be used to solve this nonlinear equation for all fixed  $p$ . We then deduce the enthalpy at saturation for each phase

$$h_\kappa^s(p) = q_\kappa + \gamma_\kappa c_{v_\kappa} T^s(p).$$

**Density** The density is linked to the enthalpy by relation (12) where

$$\rho_\kappa(h, p) = \frac{\gamma_\kappa}{\gamma_\kappa - 1} \frac{p + \pi_\kappa}{h - q_\kappa}, \quad (19a)$$

$$\rho_\kappa^s(p) = \frac{p + \pi_\kappa}{(\gamma_\kappa - 1)c_{v_\kappa} T^s(p)}. \quad (19b)$$

**Temperature** The temperature satisfies relation (13) with

$$T_\kappa(h, p) = \frac{h - q_\kappa}{\gamma_\kappa c_{v_\kappa}}.$$

**Compressibility coefficient** Relation (14) provides the expression of the compressibility coefficient with

$$\beta_\kappa(h, p) = \frac{\gamma_\kappa - 1}{\gamma_\kappa} \frac{p}{p + \pi_\kappa}.$$

We notice that  $\beta_\kappa$  is independent from  $h$  whereas  $\beta$  depends on  $h$  through the choice of the phase  $\kappa \in \{\ell, m, g\}$ .

**Remark 5.** If we define  $q$  as

$$q(h, p) = \begin{cases} q_\ell, & \text{if } h \leq h_\ell^s(p), \\ q_m \stackrel{\text{def}}{=} \left[ \frac{\rho_g^s h_g^s - \rho_\ell^s h_\ell^s}{\rho_g^s - \rho_\ell^s} \right] (p), & \text{if } h_\ell^s(p) < h < h_g^s(p), \\ q_g, & \text{if } h \geq h_g^s(p), \end{cases}$$

and given relations (12) and (14), the density can be expressed as

$$\rho(h, p) = \frac{p/\beta(h, p)}{h - q(h, p)}$$

and equation (1b) can be rewritten as

$$\partial_t h + v \partial_y h = \frac{\beta(h, p_0)}{p_0} (h - q(h, p_0)) \Phi. \quad (20)$$

We recall that  $h - q(h, p_0) > 0$  for all  $p_0$  according to Remark 4.

**Speed of sound** To compute the speed of sound  $c^*$  in a pure phase using (16a), we need to express the enthalpy  $h$  as a function of the density  $\rho$  and the pressure  $p$ . Inverting (19a) for  $\kappa \in \{\ell, g\}$ , we obtain

$$h_\kappa(\rho, p) = q_\kappa + \frac{\gamma_\kappa(p + \pi_\kappa)}{\rho(\gamma_\kappa - 1)}$$

so that (16a) becomes

$$c_\kappa^*(\rho, p) = \sqrt{\frac{\gamma_\kappa(p + \pi_\kappa)}{\rho}}.$$

In the mixture, the speed of sound satisfies equation (16b) which is written as

$$(c_m^*(h, p))^2 = \frac{h - q_m}{[-\alpha(\rho_g^s)' + (1 - \alpha)(\rho_\ell^s)']q_m + \alpha(\rho_g^s h_g^s)' + (1 - \alpha)(\rho_\ell^s h_\ell^s)' - 1}.$$

In this expression, we introduced the following notations

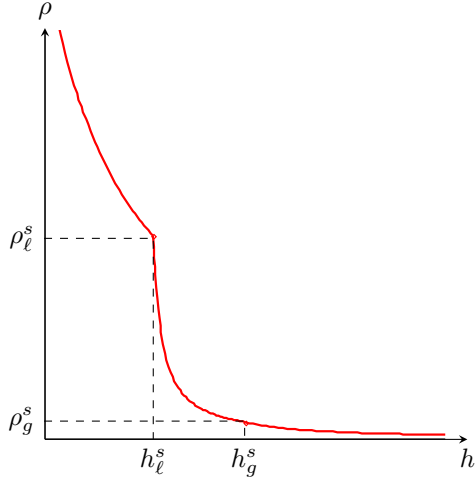
$$\begin{aligned} (\rho_\kappa^s)'(p) &= \frac{1}{(\gamma_\kappa - 1)c_{v_\kappa} T^s(p)} \left( 1 - (p + \pi_\kappa) \frac{(T^s)'}{T^s}(p) \right), \\ (\rho_\kappa^s h_\kappa^s)'(p) &= \frac{1}{(\gamma_\kappa - 1)c_{v_\kappa} T^s(p)} \left( q_\kappa + \gamma_\kappa c_{v_\kappa} T^s(p) - (p + \pi_\kappa) q_\kappa \frac{(T^s)'}{T^s}(p) \right), \\ (T^s)'(p) &= \frac{\frac{(\gamma_g - 1)c_{v_g}}{p + \pi_g} - \frac{(\gamma_\ell - 1)c_{v_\ell}}{p + \pi_\ell}}{(c_{v_\ell} \gamma_\ell - c_{v_g} \gamma_g) + \frac{q_\ell - q_g}{T^s(p)}} T^s(p). \end{aligned}$$

Graphs of density, temperature, compressibility coefficient and speed of sound for liquid water and steam at  $p = 155 \times 10^5$  Pa with parameters of Table 1 (page 40) are pictured on Figure 3.

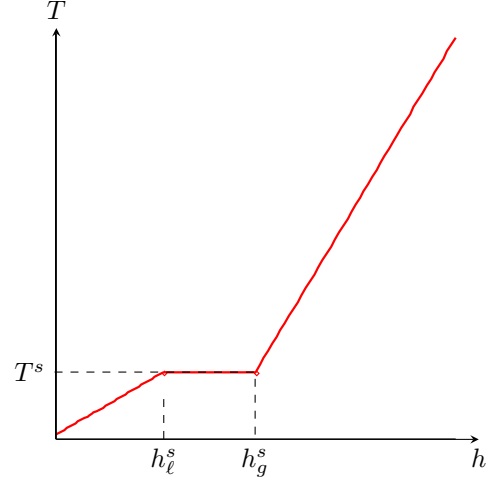
We must emphasize that as the pressure variable  $p$  is supposed to be constant and equal to  $p_0$  in the LMNC model, most parameters are constant throughout the study (such as  $T^s$ ,  $\beta_\kappa$  or  $q_\kappa$ ). That is why references to the dependence on the pressure may be dropped in the sequel for the sake of simplicity.

### 3 Theoretical study

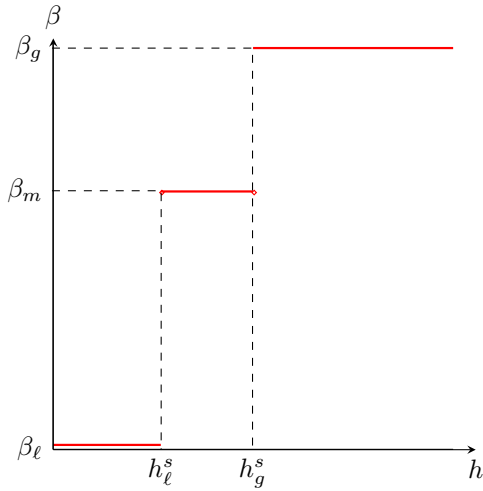
In this section we derive some analytical steady and unsteady solutions to system (1). For a single phase flow we obtain exact and asymptotic solutions for different power densities and inlet velocities. We then generalize these calculations to two-phase flows with phase transition.



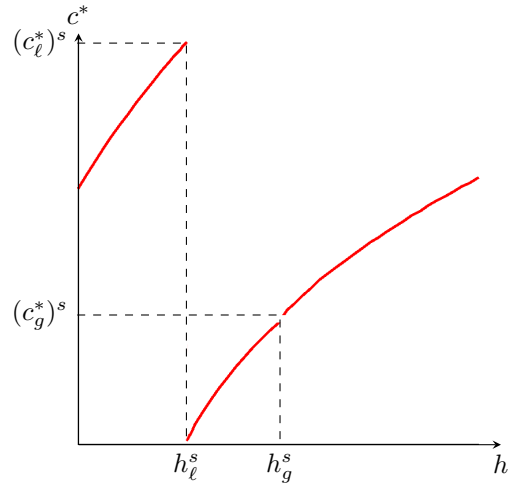
(a) Density as a function of the enthalpy: the densities of the liquid phase and the vapor phase at saturation are  $\rho_\ell^s \approx 632.663 \text{ kg} \cdot \text{m}^{-3}$  and  $\rho_g^s \approx 52.937 \text{ kg} \cdot \text{m}^{-3}$ .



(b) Temperature as a function of the enthalpy: the temperature at saturation is  $T^s \approx 654 \text{ K}$ .



(c) Compressibility coefficient as a function of the enthalpy: the compressibility coefficients of the liquid phase, the mixture at saturation and the vapor phase are  $\beta_\ell \approx 0.008769$ ,  $\beta_m \approx 0.194852$  and  $\beta_g \approx 0.300699$ .



(d) Speed of sound as a function of the enthalpy: the speed of sound of the liquid phase and the vapor phase at saturation are  $(c_\ell^*)^s \approx 1942 \text{ m} \cdot \text{s}^{-1}$  and  $(c_g^*)^s \approx 647 \text{ m} \cdot \text{s}^{-1}$ ; in the mixture at saturation the speed of sound is in the range  $(78 \text{ m} \cdot \text{s}^{-1}, 631 \text{ m} \cdot \text{s}^{-1})$ .

Figure 3: EOS with phase transition for parameters of Table 1 at page 40 with  $p_0 = 155 \times 10^5 \text{ Pa}$ : the enthalpies of the liquid phase and the vapor phase at saturation are  $h_\ell^s \approx 1.627 \times 10^6 \text{ J} \cdot \text{K}^{-1}$  and  $h_g^s \approx 3.004 \times 10^6 \text{ J} \cdot \text{K}^{-1}$ .

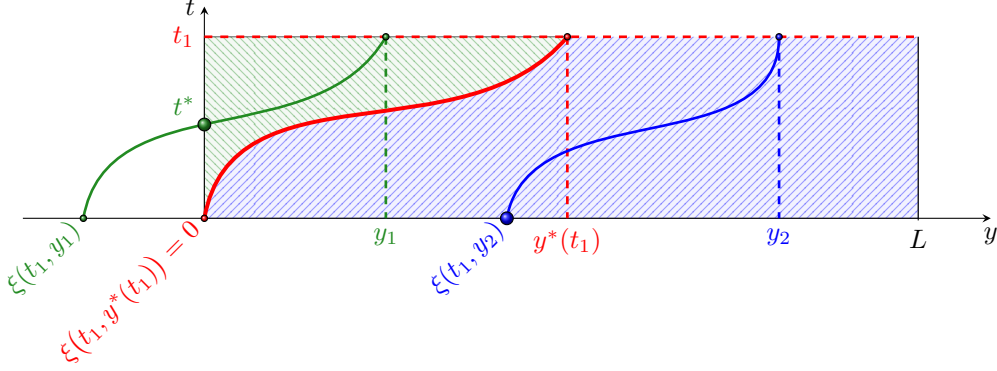


Figure 4: Sketch of the method of characteristics and definitions of  $\xi(t, y)$  and  $t^*(t, y)$ .

### 3.1 Exact and asymptotic solutions for single-phase flow

In this section we compute some analytical solutions of (1) supplemented with the stiffened gas law for some particular cases (according to  $\Phi$  and  $v_e$ ) when a single phase  $\kappa \in \{\ell, m, g\}$  is present. The compressibility coefficient  $\beta$  and the coefficient  $q$  are thus constant. The following results have first been stated in [3]. The proofs are detailed therein.

Since we focus on the 1D case, we can compute the velocity  $v$  by a direct integration of equation (1a), which gives

$$v(t, y) = v_e(t) + \frac{\beta_\kappa}{p_0} \int_0^y \Phi(t, z) dz. \quad (21)$$

This velocity is obviously non-negative under Hypotheses 1, 2 and 3, so that system (1) is well-posed. As mentioned earlier, equation (1b) can be rewritten as (20). We can thus apply the method of characteristics to compute the enthalpy.

#### 3.1.1 Constant power density

**Proposition 3.** *Assume the power density  $\Phi = \Phi_0$  and the inlet velocity  $v_e$  constant in time and space and denote  $\hat{\Phi}_0 \stackrel{\text{def}}{=} \beta_\kappa \Phi / p_0$ . Let  $\xi(t, y)$  and  $t^*(t, y)$  be defined as follows*

$$\begin{aligned} \xi(t, y) &\stackrel{\text{def}}{=} \left( y + \frac{v_e}{\hat{\Phi}_0} \right) e^{-\hat{\Phi}_0 t} - \frac{v_e}{\hat{\Phi}_0}, \\ t^*(t, y) &\stackrel{\text{def}}{=} t - \frac{1}{\hat{\Phi}_0} \ln \left( 1 + \frac{\hat{\Phi}_0 y}{v_e} \right) = -\frac{1}{\hat{\Phi}_0} \ln \left( 1 + \frac{\hat{\Phi}_0}{v_e} \xi(t, y) \right). \end{aligned}$$

Then the solution  $h$  of equation (1b) is given by

$$h(t, y) = \begin{cases} q_\kappa + [h_0(\xi(t, y)) - q_\kappa] e^{\hat{\Phi}_0 t}, & \text{if } \xi(t, y) \geq 0, \\ q_\kappa + [h_e(t^*(t, y)) - q_\kappa] \left( 1 + \frac{\hat{\Phi}_0 y}{v_e} \right) = h_e(t^*(t, y)) + \frac{\Phi_0 y}{D_e(t^*(t, y))}, & \text{if } \xi(t, y) < 0. \end{cases} \quad (22)$$

**Corollary 1.** *The solution  $\bar{p}$  of equation (1c) is given by*

- if  $\xi(t, y) \geq 0$  then

$$\begin{aligned} \bar{p}(t, y) = & \hat{\Phi}_0[\mu(y) - \mu(L)] + \\ & \frac{p_0}{\beta_\kappa} \left\{ \beta_\kappa + \left( g + \hat{\Phi}_0 v_e e^{\hat{\Phi}_0 t} \right) [\bar{H}_0(\xi(t, L)) - \bar{H}_0(\xi(t, y))] \right. \\ & \left. + \hat{\Phi}_0^2 e^{\hat{\Phi}_0 t} [\bar{\bar{H}}_0(\xi(t, L)) - \bar{\bar{H}}_0(\xi(t, y))] \right\}, \end{aligned} \quad (23a)$$

- otherwise

$$\begin{aligned} \bar{p}(t, y) = & \hat{\Phi}_0[\mu(y) - \mu(L)] + \\ & \frac{p_0}{\beta_\kappa} \left\{ \beta_\kappa + \left( g + \hat{\Phi}_0 v_e e^{\hat{\Phi}_0 t} \right) [\bar{H}_0(\xi(t, L)) - \bar{H}_0(0)] + \hat{\Phi}_0^2 e^{\hat{\Phi}_0 t} [\bar{\bar{H}}_0(\xi(t, L)) - \bar{\bar{H}}_0(0)] \right. \\ & \left. - v_e \left( g + \hat{\Phi}_0 v_e e^{\hat{\Phi}_0 t} \right) [\bar{H}_e(0) - \bar{H}_e(t^*(t, y))] - \hat{\Phi}_0 v_e^2 [\bar{\bar{H}}_e(0) - \bar{\bar{H}}_e(t^*(t, y))] \right\}, \end{aligned} \quad (23b)$$

where  $\bar{H}_0$ ,  $\bar{\bar{H}}_0$ ,  $\bar{H}_e$  and  $\bar{\bar{H}}_e$  are respectively some primitive functions of  $y \mapsto 1/(h_0(y) - q)$ ,  $y \mapsto y/(h_0(y) - q)$ ,  $t \mapsto 1/(h_e(t) - q)$  and  $t \mapsto e^{-\hat{\Phi}_0 t}/(h_e(t) - q)$ .

*Proof of Proposition 3.* Equation (21) becomes

$$v(t, y) = v_e + \hat{\Phi}_0 y. \quad (24)$$

Given this velocity field, we introduce the characteristic curves: let  $\chi(\tau; t, y)$  be the position at time  $\tau$  of a particle located in  $y$  at time  $t$  in a flow driven at velocity  $v$ . Hence  $\chi$  is solution to the parametrized ODE for  $t \geq 0$  and  $y \in (0, L)$

$$\begin{cases} \frac{d\chi}{d\tau}(\tau; t, y) = v(\tau, \chi(\tau; t, y)), & (25a) \\ \chi(t; t, y) = y. & (25b) \end{cases}$$

Since  $v$  is linear, the Cauchy-Lipschitz theorem ensures the existence of  $\chi$  over some interval (depending on  $t$  and  $y$ ). Moreover,  $\chi$  is continuous with respect to  $(\tau, t, y)$ . We then solve ODE (25) using expression (24). We obtain

$$\chi(\tau; t, y) = \left( y + \frac{v_e}{\hat{\Phi}_0} \right) e^{\hat{\Phi}_0(\tau-t)} - \frac{v_e}{\hat{\Phi}_0}.$$

Let us now explain the two notations introduced in the statement of the proposition.  $\xi(t, y)$  corresponds to the foot of the characteristic curve passing at the point  $(t, y)$ , *i.e.*  $\xi(t, y) = \chi(0; t, y)$ . When  $\xi(t, y) \leq 0$ ,  $t^*(t, y)$  is the time at which the characteristic curve crosses the boundary  $y = 0$ , *i.e.* the solution of the equation  $\chi(t^*; t, y) = 0$  (see Figure 4). For fixed  $t \geq 0$  and  $y \in (0, L)$ , the requirement  $\chi(\tau; t, y) \in (0, L)$  constrains the interval of existence

$$\tau \in \left( \max \{0; t^*(t, y)\}, t + \frac{1}{\hat{\Phi}_0} \ln \left( \frac{v_e + \hat{\Phi}_0 L}{v_e + \hat{\Phi}_0 y} \right) \right). \quad (26)$$

For  $(\tau, t, y)$  satisfying (26), we note

$$\hat{h}(\tau; t, y) \stackrel{\text{def}}{=} h(\tau; \chi(\tau; t, y)). \quad (27)$$

We deduce from equation (20) that  $\hat{h}$  satisfies

$$\begin{cases} \partial_\tau [\hat{h}(\tau; t, y) - q_\kappa] = \hat{\Phi}_0 [\hat{h}(\tau; t, y) - q_\kappa], \\ \hat{h}(t; t, y) = h(t, y). \end{cases}$$

The solution of this linear first order ODE is

$$h(t, y) - q_\kappa = \hat{h}(t; t, y) - q_\kappa = [\hat{h}(\tau; t, y) - q_\kappa] e^{\hat{\Phi}_0(t-\tau)} = [h(\tau; \chi(\tau; t, y)) - q_\kappa] e^{\hat{\Phi}_0(t-\tau)}. \quad (28)$$

Two cases must be investigated depending on the minimal time until which the characteristic curve remains in the domain or equivalently depending on the sign of  $\xi$  (see (26) and Figure 4):

- if  $\xi(t, y) \geq 0$ , then the characteristic curve does not cross the boundary  $y = 0$ , which means that we can take  $\tau = 0$  in equation (28) and

$$h(t, y) - q_\kappa = [h_0(\chi(0; t, y)) - q_\kappa] e^{\hat{\Phi}_0 t} = [h_0(\xi(t, y)) - q_\kappa] e^{\hat{\Phi}_0 t};$$

- if  $\xi(t, y) < 0$ , the backward characteristic curve reaches the boundary at time  $t^*(t, y) > 0$  and

$$h(t, y) - q_\kappa = (h_e(t^*) - q_\kappa) e^{\hat{\Phi}_0(t-t^*)} = (h_e(t^*) - q_\kappa) \left(1 + \frac{\hat{\Phi}_0 y}{v_e}\right).$$

Noticing that  $h - q_\kappa = \frac{p_0}{\beta_\kappa} \frac{1}{\rho}$  leads to

$$h(t, y) = q_\kappa + (h_e(t^*) - q_\kappa) + \frac{1}{\rho_e(t^*)} \frac{\Phi_0}{v_e} y = h_e(t^*) + \frac{\Phi_0}{D_\epsilon(t^*)} y.$$

□

*Proof of Corollary 1.* The exact dynamic pressure  $\bar{p}$  can be computed by integrating the momentum equation (1c) which is equivalent to

$$\partial_y \bar{p} = -\partial_t(\rho v) - \partial_y(\rho v^2) + \partial_y(\mu \partial_y v) - \rho g.$$

Using the mass conservation law and observing that  $v$  given by (24) is independent of time, we obtain

$$\partial_y \bar{p} = -(\hat{\Phi}_0 v + g)\rho + \hat{\Phi}_0 \partial_y \mu$$

from which we deduce

$$\partial_y \bar{p} = -\frac{p_0}{\beta_\kappa} \frac{g + \hat{\Phi}_0(v_e + \hat{\Phi}_0 y)}{h - q_\kappa} + \hat{\Phi}_0 \partial_y \mu.$$

Integrating between  $y$  and  $L$ , we get

$$\bar{p}(t, y) = p_0 + \frac{p_0(g + \hat{\Phi}_0 v_e)}{\beta_\kappa} \int_y^L \frac{1}{H(t, z)} dz + \frac{p_0 \hat{\Phi}_0^2}{\beta_\kappa} \int_y^L \frac{z}{H(t, z)} dz + \hat{\Phi}_0 [\mu(y) - \mu(L)]$$

where  $H \stackrel{\text{def}}{=} h - q_\kappa$ . Since  $h$  is defined piecewise by (22), we have to consider two cases:

- if  $\xi(t, y) \geq 0$ , we have  $H(t, y) = H_0(\xi(t, y)) e^{\hat{\Phi}_0 t}$  so that by means of the change of variable  $\zeta = \xi(t, z)$  we can compute each integral

$$\int_y^L \frac{1}{H(t, z)} dz = \int_{\xi(t, y)}^{\xi(t, L)} \frac{1}{H_0(\zeta)} d\zeta = [\overline{H_0}(\zeta)]_{\xi(t, y)}^{\xi(t, L)},$$

$$\begin{aligned}
\int_y^L \frac{z}{H(z)} dz &= \int_{\xi(t,y)}^{\xi(t,L)} \frac{\xi^{-1}(t,\zeta)}{H_0(\zeta)} d\zeta \\
&= e^{\hat{\Phi}_0 t} \int_{\xi(t,y)}^{\xi(t,L)} \frac{\zeta}{H_0(\zeta)} d\zeta + (e^{\hat{\Phi}_0 t} - 1) \frac{v_e}{\hat{\Phi}_0} \int_{\xi(t,y)}^{\xi(t,L)} \frac{1}{H_0(\zeta)} d\zeta \\
&= e^{\hat{\Phi}_0 t} \left[ \overline{H_0}(\zeta) \right]_{\xi(t,y)}^{\xi(t,L)} + (e^{\hat{\Phi}_0 t} - 1) \frac{v_e}{\hat{\Phi}_0} \left[ \overline{H_0}(\zeta) \right]_{\xi(t,y)}^{\xi(t,L)}.
\end{aligned}$$

Hence we deduce (23a).

- if  $\xi(t, y) < 0$ , we have  $H(t, y) = \left(1 + \frac{\hat{\Phi}_0}{v_e} y\right) H_e(t^*(t, y))$ . The integration domain is split into two parts depending on the sign of  $\xi(t, z)$ . More precisely

$$\int_y^L f(z) dz = \int_{y^*(t)}^L f(z) dz + \int_y^{y^*(t)} f(z) dz$$

for any function  $f$  and with  $y^*(t) \stackrel{\text{def}}{=} (e^{\hat{\Phi}_0 t} - 1) \frac{v_e}{\hat{\Phi}_0}$  (see Figure 4). For integrals between  $y^*(t)$  and  $L$ , we apply the previous result with  $y = y^*(t)$ . For integrals between  $y$  and  $y^*(t)$ , we use the change of variables  $\zeta = t - \frac{1}{\hat{\Phi}_0} \ln \left(1 + \frac{\hat{\Phi}_0}{v_e} z\right)$

$$\begin{aligned}
\int_y^{y^*(t)} \frac{1}{H(t, z)} dz &= -v_e \int_{t^*(t,y)}^0 \frac{1}{H_e(\zeta)} d\zeta = v_e \left[ \overline{H_e}(\zeta) \right]_0^{t^*(t,y)}, \\
\int_y^{y^*(t)} \frac{z}{H(t, z)} dz &= \frac{v_e^2}{\hat{\Phi}_0} \int_0^{t^*(t,y)} \frac{e^{\hat{\Phi}_0(t-\zeta)} - 1}{H_e(\zeta)} d\zeta = \frac{v_e^2}{\hat{\Phi}_0} \left[ (e^{\hat{\Phi}_0 t} - 1) \overline{H_e}(\zeta) + \overline{H_e}(\zeta) \right]_0^{t^*(t,y)}.
\end{aligned}$$

Summing all terms leads to (23b). □

**Remark 6.** As it has been stated in [3], if the inlet enthalpy is also constant and if the inlet velocity is nonzero, there is an asymptotic state which is reached in finite time. It is given by

$$v^\infty(y) = v_e + \hat{\Phi}_0 y, \quad h^\infty(y) = h_e + \frac{\Phi_0}{D_e} y.$$

However, if the inlet velocity is  $v_e = 0$ , then  $\xi(t, y)$  is always positive and no asymptotic state can be reached since the enthalpy increases continuously in time.

### 3.1.2 Varying power density (with $t$ or $y$ )

**Proposition 4.** Assume the power density  $\Phi$  depends on space and the inlet velocity  $v_e$  is independent of time. Let us define

$$\Theta(y) \stackrel{\text{def}}{=} \int_0^y \frac{dz}{v(z)}, \quad \xi(t, y) \stackrel{\text{def}}{=} \Theta^{-1}(\Theta(y) - t) \quad \text{and} \quad t^*(t, y) \stackrel{\text{def}}{=} t - \Theta(y).$$

Then the solution  $h$  of equation (1b) is given by

$$h(t, y) = \begin{cases} q_\kappa + v(y) \frac{h_0(\xi(t, y)) - q_\kappa}{v(\xi(t, y))}; & \text{if } \xi(t, y) \geq 0, \\ q_\kappa + v(y) \frac{h_e(t^*(t, y)) - q_\kappa}{v_e} = h_e(t^*(t, y)) + \frac{1}{D_e(t^*(t, y))} \int_0^y \Phi(z) dz, & \text{if } \xi(t, y) < 0. \end{cases}$$

*Proof.* Since the inlet velocity  $v_e$  is a positive constant, the velocity  $v(t, y) = v(y)$  is a positive function and  $\Theta$  is thus invertible. In a similar way as for the previous proposition, we solve the characteristic ODE (25) which leads to  $\Theta(\chi(\tau)) - \Theta(y) = \tau - t$  and

$$\chi(\tau; t, y) = \Theta^{-1}(\Theta(y) + \tau - t). \quad (29)$$

We can ensure that  $\chi(\tau; t, y) \in (0, L)$  provided  $\tau \in (\max\{0, t^*(t, y)\}, t + \Theta(L) - \Theta(y))$ . Keeping the same notation (27) for  $\hat{h}$ , equation (20) becomes

$$\begin{cases} \partial_\tau [\hat{h}(\tau; t, y) - q_\kappa] = \frac{\beta_\kappa}{p_0} [\hat{h}(\tau; t, y) - q_\kappa] \Phi(\chi(\tau; t, y)), \\ \hat{h}(t; t, y) = h(t, y). \end{cases} \quad (30)$$

For the sake of simplicity, we set  $\chi' = \frac{d\chi}{d\tau}$  and  $\chi'' = \frac{d^2\chi}{d\tau^2}$ . We differentiate ODE (25) to obtain

$$\chi''(\tau; t, y) = \chi'(\tau; t, y) \frac{dv}{dy}(\chi(\tau; t, y)) = \chi'(\tau; t, y) \frac{\beta_\kappa}{p_0} \Phi(\chi(\tau; t, y)).$$

The positivity of  $v$  implies that  $\chi'(\tau; t, y) > 0$  and

$$\frac{\beta_\kappa}{p_0} \Phi(\chi(\tau; t, y)) = \frac{\chi''(\tau; t, y)}{\chi'(\tau; t, y)} = [\ln(\chi'(\tau; t, y))] = [\ln v(\chi(\tau; t, y))]'.$$

Inserting this relation in equation (30), we have

$$\partial_\tau(\hat{h} - q_\kappa) = (\hat{h} - q_\kappa) \partial_\tau [\ln v(\chi(\tau; t, y))].$$

Hence

$$h(t, y) - q_\kappa = v(y) \frac{h(\tau, \chi(\tau; t, y)) - q_\kappa}{v(\chi(\tau; t, y))}.$$

Given expression (29) for  $\chi$ , we finally obtain

$$h(t, y) = q_\kappa + \begin{cases} v(y) \frac{h_0(\xi(t, y)) - q_\kappa}{v(\xi(t, y))}, & \text{if } \xi(t, y) \geq 0, \\ v(y) \frac{h_e(t^*(t, y)) - q_\kappa}{v_e}, & \text{otherwise.} \end{cases}$$

□

**Proposition 5.** *Assume the power density  $\Phi$  only depends on time. We define*

$$\Psi(t) \stackrel{\text{def}}{=} \frac{\beta_\kappa}{p_0} \int_0^t \Phi(s) ds \quad \text{and} \quad \xi(t, y) \stackrel{\text{def}}{=} ye^{-\Psi(t)} - \int_0^t v_e(s) e^{-\Psi(s)} ds.$$

*Let  $t^*(t, y)$  be the solution of the equation (in  $t$ )  $y = \int_{t^*}^t v_e(s) e^{\Psi(t) - \Psi(s)} ds$ . Then the solution  $h$  of equation (1b) is given by*

$$h(t, y) = q_\kappa + \begin{cases} [h_0(\xi(t, y)) - q_\kappa] e^{\Psi(t)}, & \text{if } \xi(t, y) \geq 0, \\ [h_e(t^*(t, y)) - q_\kappa] e^{\Psi(t) - \Psi(t^*)}, & \text{if } \xi(t, y) < 0. \end{cases}$$

*Proof.* As previously, the key point is the integration of the characteristic ODE (25) which reads

$$\frac{d}{d\tau} \left( \chi(\tau) e^{-\Psi(\tau)} \right) = v_e(\tau) e^{-\Psi(\tau)}.$$

This leads to

$$\chi(\tau; t, y) = y e^{\Psi(t) - \Psi(\tau)} + \int_t^\tau v_e(s) e^{\Psi(t) - \Psi(s)} ds.$$

Consequently

$$h(t, y) - q_\kappa = [h(\tau, \chi(\tau; t, y)) - q_\kappa] e^{\Psi(t) - \Psi(\tau)}.$$

The main issue is then to determine the interval for  $\tau$  such that  $\chi(\tau; t, y) \in (0, L)$ . The equality  $\chi(\tau; t, y) = 0$  can be rewritten as

$$y = \int_\tau^t v_e(s) e^{\Psi(t) - \Psi(s)} ds.$$

As the right hand side vanishes for  $\tau = t$ , two cases may occur: either  $y$  is greater than the right hand side for  $\tau = 0$  (which would imply that the left bound of the interval is 0), or there exists  $\tau = t^* > 0$  such that the previous equality holds. In the former case, we obtain

$$h(t, y) - q_\kappa = [h_0(\chi(0; t, y)) - q_\kappa] e^{\Psi(t)},$$

while in the latter case

$$h(t, y) - q_\kappa = [h_e(t^*(t, y)) - q_\kappa] e^{\Psi(t) - \Psi(t^*)}.$$

□

**Remark 7.** *In the general case, i.e. with time dependence for  $h_e$  and  $D_e$  and time/space dependence for  $\Phi$ , it does not seem possible to compute an exact solution. However, if  $h_e(t)$ ,  $D_e(t)$  and  $\Phi(t, y)$  have a finite limit as  $t \rightarrow +\infty$  denoted by  $h_e^\infty$ ,  $D_e^\infty$ ,  $\Phi^\infty(y)$ , then there exists an asymptotic solution for the enthalpy*

$$h^\infty(y) = h_e^\infty + \frac{1}{D_e^\infty} \int_0^y \Phi^\infty(z) dz$$

and all other quantities are deduced from  $h^\infty$ . We recover the results of [12].

### 3.2 Exact and asymptotic solutions for two-phase flow with phase transition

In the case of a two-phase flow with phase transition and if we can determine the position of each phase, we can deduce the exact solution using the single-phase flow results given in Section 3.1. In the particular case where all parameters and boundary/initial data are constant, the result is the following.

**Proposition 6.** *Let us assume that the inlet enthalpy  $h_e$ , the inlet velocity  $v_e$ , the power density  $\Phi_0$  and the initial enthalpy  $h_0$  are constant. Let  $\hat{\Phi}_\kappa \stackrel{\text{def}}{=} \beta_\kappa \Phi_0 / p_0$ , where  $\kappa$  is respectively  $\ell$ ,  $m$ ,  $g$  in the liquid, mixture and gas phase. We suppose that the initial and boundary data correspond to the liquid phase, i.e.  $h_e = h_0 < h_\ell^s$ . We set*

$$y_\ell^s \stackrel{\text{def}}{=} \frac{D_e}{\hat{\Phi}_0} (h_\ell^s - h_e), \quad t_\ell^s \stackrel{\text{def}}{=} \frac{1}{\hat{\Phi}_\ell} \ln \left( \frac{h_\ell^s - q_\ell}{h_0 - q_\ell} \right),$$

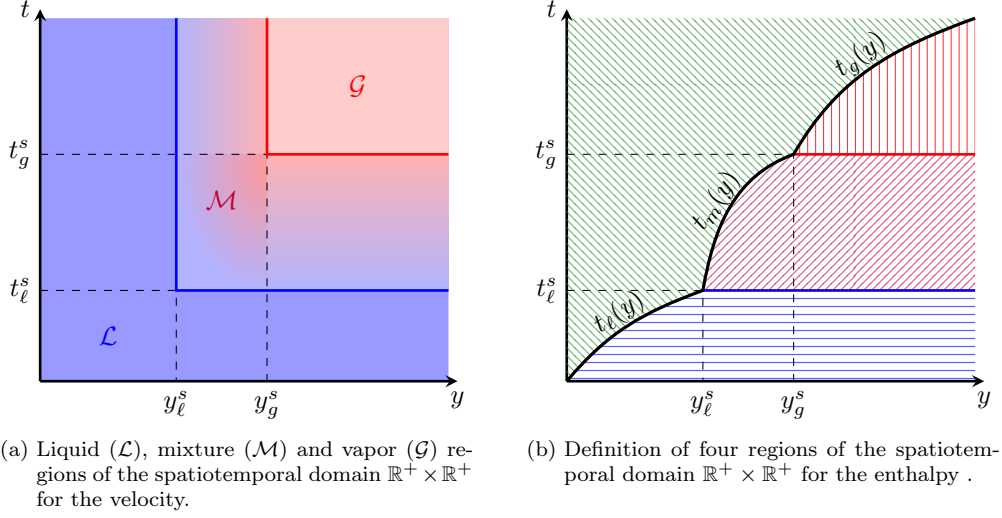


Figure 5: Definition of regions for Proposition 6

$$y_g^s \stackrel{\text{def}}{=} \frac{D_e}{\Phi_0} (h_g^s - h_e), \quad t_g^s \stackrel{\text{def}}{=} t_\ell^s + \frac{1}{\hat{\Phi}_m} \ln \left( \frac{h_g^s - q_m}{h_\ell^s - q_m} \right).$$

Let us define three curves in  $\mathbb{R}^+ \times \mathbb{R}^+$  as pictured on Figure 5b

$$\begin{aligned} t_\ell(y) &\stackrel{\text{def}}{=} \frac{1}{\hat{\Phi}_\ell} \ln \left( 1 + \frac{\hat{\Phi}_\ell y}{v_e} \right), & \text{for } 0 \leq y \leq y_\ell^s, \\ t_m(y) &\stackrel{\text{def}}{=} \frac{1}{\hat{\Phi}_m} \ln \left( \frac{v_e + (\hat{\Phi}_\ell - \hat{\Phi}_m)y_\ell^s + \hat{\Phi}_m y}{v_e + \hat{\Phi}_\ell y_\ell^s} \right) + t_\ell(y_\ell^s), & \text{for } y_\ell^s < y < y_g^s, \\ t_g(y) &\stackrel{\text{def}}{=} \frac{1}{\hat{\Phi}_g} \ln \left( \frac{v_e + (\hat{\Phi}_\ell - \hat{\Phi}_m)y_\ell^s + (\hat{\Phi}_m - \hat{\Phi}_g)y_g^s + \hat{\Phi}_g y}{v_e + (\hat{\Phi}_\ell - \hat{\Phi}_m)y_\ell^s + \hat{\Phi}_m y_g^s} \right) + t_m(y_g^s), & \text{for } y \geq y_g^s. \end{aligned}$$

Then the spatiotemporal domain  $\mathbb{R}^+ \times \mathbb{R}^+$  consists of three regions corresponding to liquid, mixture and vapor phases as follows (see Figure 5a):

$$\begin{aligned} \mathcal{L} &= \{ (t, y) \in \mathbb{R}^+ \times \mathbb{R}^+ \mid t \leq t_\ell^s \text{ or } y \leq y_\ell^s \}, \\ \mathcal{M} &= \{ (t, y) \in (t_\ell^s, +\infty) \times (y_\ell^s, +\infty) \mid t \leq t_g^s \text{ or } y \leq y_g^s \}, \\ \mathcal{G} &= \{ (t, y) \in (t_g^s, +\infty) \times (y_g^s, +\infty) \}; \end{aligned}$$

the solution  $v$  of equation (1a) is given by

$$v(t, y) = \begin{cases} v_e + \hat{\Phi}_\ell y, & \text{if } (t, y) \in \mathcal{L}, \\ v_e + \hat{\Phi}_\ell y_\ell^s + \hat{\Phi}_m (y - y_\ell^s), & \text{if } (t, y) \in \mathcal{M}, \\ v_e + \hat{\Phi}_\ell y_\ell^s + \hat{\Phi}_m (y_g^s - y_\ell^s) + \hat{\Phi}_g (y - y_g^s), & \text{if } (t, y) \in \mathcal{G}, \end{cases}$$

and the solution  $h$  of equation (1b) is given by (see Figure 5b)

$$h(t, y) = \begin{cases} q_\ell + (h_0 - q_\ell)e^{\hat{\Phi}_\ell t}, & \text{if } (t, y) \in \mathcal{L} \text{ and } t < t_\ell(y), \\ q_m + (h_\ell^s - q_m)e^{\hat{\Phi}_m(t-t_\ell^s)}, & \text{if } (t, y) \in \mathcal{M} \text{ and } t < t_m(y), \\ q_g + (h_g^s - q_g)e^{\hat{\Phi}_g(t-t_g^s)}, & \text{if } (t, y) \in \mathcal{G} \text{ and } t < t_g(y), \\ h_e + \frac{\Phi_0}{D_e}y, & \text{otherwise.} \end{cases}$$

*Proof.* Since  $\rho_e, v_e, h_0$  and  $\Phi_0$  are constant and correspond to the liquid phase, equations (1a)-(1b) are written over a time interval  $[0, \mathcal{T})$  for some  $\mathcal{T} > 0$  to be specified later (which corresponds to the first time another phase appears)

$$\begin{cases} \partial_y v = \hat{\Phi}_\ell, \\ \partial_t h + v \partial_y h = \hat{\Phi}_\ell(h - q_\ell), \\ v(t, 0) = v_e, \\ h(t, 0) = h_e, \\ h(0, t) = h_0 = h_e. \end{cases}$$

We can apply Proposition 3 to this system which leads to

$$v(y) = v_e + \hat{\Phi}_\ell y$$

and

$$h(t, y) = \begin{cases} q_\ell + (h_0 - q_\ell)e^{\hat{\Phi}_\ell t}, & \text{if } t < t_\ell(y), \\ h_e + \frac{\Phi_0}{D_e}y, & \text{otherwise,} \end{cases}$$

where the curve  $t = t_\ell(y)$  corresponds to the characteristic curve coming from  $(t = 0, y = 0)$ . The enthalpy  $h(t, \cdot)$  is a monotone-increasing function consisting (spatially) of a linear part and a constant part at each time. Two situations may occur:

- either  $h_e + \frac{\Phi_0}{D_e}L \leq h_\ell^s$ : the fluid remains liquid indefinitely ( $\mathcal{T} = +\infty$ ) and the enthalpy is equal to  $h_e + \frac{\Phi_0}{D_e}y$  everywhere as soon as  $t \geq t_\ell(L)$ ;
- or  $h_e + \frac{\Phi_0}{D_e}L < h_\ell^s$ : a mixture phase appears.

In the latter case, there exists  $t > 0$  and  $y \in (0, L)$  such that  $h(t, y) = h_\ell^s$ . We then define  $\mathcal{T} = t_\ell^s$  as the solution of  $h(t_\ell^s, L) = h_\ell^s$  and  $y_\ell^s$  as the smallest  $y$  such that  $h(t_\ell^s, y) = h_\ell^s$ , i.e.

$$q_\ell + (h_0 - q_\ell)e^{\hat{\Phi}_\ell t_\ell^s} = h_\ell^s, \quad h_e + \frac{\Phi_0}{D_e}y_\ell^s = h_\ell^s.$$

We mention that  $t_\ell^s = t_\ell(y_\ell^s)$ . For  $t > t_\ell^s$ , the fluid is in liquid phase for  $y < y_\ell^s$  and in mixture phase for  $y \geq y_\ell^s$ . Therefore, in the liquid region the previous solution is still valid, whereas in the mixture region  $[t_\ell^s, \mathcal{T}') \times [y_\ell^s, L]$  equations (1a)-(1b) are written as

$$\begin{cases} \partial_y v = \hat{\Phi}_m, \\ \partial_t h + v \partial_y h = \hat{\Phi}_m(h - q_m), \\ v(t, y_\ell^s) = v_e + \hat{\Phi}_\ell y_\ell^s, \\ h(t, y_\ell^s) = h_\ell^s, \\ h(t_\ell^s, y) = h_\ell^s. \end{cases}$$

We adapt Proposition 3 to the current spatiotemporal domain so that we obtain

$$v(y) = v_e + \hat{\Phi}_\ell y_\ell^s + \hat{\Phi}_m (y - y_\ell^s)$$

and

$$h(t, y) = \begin{cases} q_m + (h_\ell^s - q_m) e^{\hat{\Phi}_m (t - t_\ell^s)}, & \text{if } t < t_m(y), \\ h_e + \frac{\Phi}{D_e} y, & \text{otherwise.} \end{cases}$$

The curve  $t = t_m(y)$  corresponds to the characteristic curve passing through  $(t_\ell^s, y_\ell^s)$ , *i.e.*

$$t_m(y) = \frac{1}{\hat{\Phi}_m} \ln \left( \frac{v_e + (\hat{\Phi}_\ell - \hat{\Phi}_m) y_\ell^s + \hat{\Phi}_m y}{v_e + \hat{\Phi}_\ell y_\ell^s} \right) + t_\ell^s.$$

This can be rewritten in a simpler form. To this end, we use the definition of  $y_\ell^s$ , the relation  $\frac{1}{\rho_e} = \frac{\beta_\ell}{p_0} (h_e - q_\ell)$  and the continuity of  $\rho$  at  $y_\ell^s$  (implying  $\beta_m (h_\ell^s - q_m) = \beta_\ell (h_\ell^s - q_\ell)$ ) which leads to

$$t_m(y) = \frac{1}{\hat{\Phi}_m} \ln \left( \frac{h_e - q_m + \frac{\Phi_0 y}{D_e}}{h_\ell^s - q_m} \right) + t_\ell^s.$$

Applying the same procedure we find  $(t_g^s, y_g^s)$  such that  $h_g^s$  is reached and the proof follows.  $\square$

The assumptions of Proposition 6 may seem restrictive but it can be trivially extended to several cases:

- to other *constant* initial and boundary conditions (*i.e.* mixture or vapor);
- if  $\Phi = \Phi_0 < 0$  but  $v$  remains positive since the enthalpy is still monotone.

If  $\Phi$  and/or boundary-initial conditions are not constant anymore, the enthalpy is no longer monotone. It is thus difficult to determine regions  $\mathcal{L}$ ,  $\mathcal{M}$  and  $\mathcal{G}$ . However, if this can be achieved, we can similarly apply the monophasic results in each region to compute the exact solution. In any case, the following result holds (similar to Remark 7):

**Proposition 7.** *For any inlet velocity  $v_e$ , inlet flow rate  $D_e$  and power density  $\Phi$  which have finite limits in time, let us denote  $(h_e^\infty, D_e^\infty, \Phi^\infty(y)) = \lim_{t \rightarrow +\infty} (h_e(t), D_e(t), \Phi(t, y))$ . Then, the asymptotic solution  $(h^\infty(y), v^\infty(y), \bar{p}^\infty(y))$  is given by*

$$\begin{aligned} h^\infty(y) &= h_e^\infty + \frac{1}{D_e^\infty} \int_0^y \Phi^\infty(z) \, dz, \\ v^\infty(y) &= \frac{D_e^\infty}{\rho(h^\infty(y), p_0)}, \\ \bar{p}^\infty(y) &= p_0 + g \int_y^L \rho(h^\infty(z), p_0) \, dz - \left[ \mu \frac{\beta(h^\infty(z), p_0) \Phi^\infty(z)}{p_0} - \frac{(D_e^\infty)^2}{\rho(h^\infty(z), p_0)} \right]_{z=y}^{z=L}. \end{aligned}$$

**Remark 8.** *Under the assumptions of Proposition 7, coefficients  $y_\ell^s$  and  $y_g^s$  can always be computed. It can thus be stated whether the fluid appears only as a liquid phase (if  $y_\ell^s > L$ ) or also as mixture ( $y_\ell^s \leq L \leq y_g^s$ ) or vapor ( $y_\ell^s < y_g^s < L$ ). In any case, we observe that a steady state is reached. It is given by*

$$h^\infty(y) = h_e + \frac{\Phi_0}{D_e} y$$

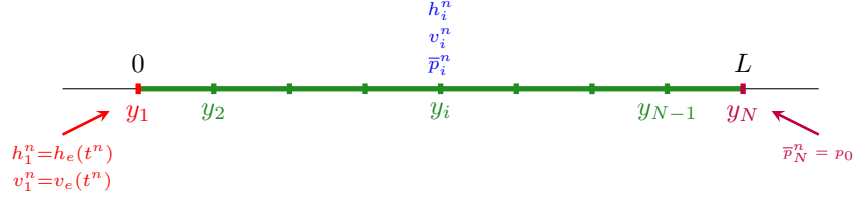


Figure 6: Grid and boundary conditions.

and the velocity is piecewise linear. Moreover, we can determine the time  $t_\infty$  at which the asymptotic state is reached

$$t_\infty \stackrel{\text{def}}{=} \begin{cases} t_\ell(L), & \text{if } y_\ell^s > L, \\ t_m(L), & \text{if } y_\ell^s \leq L \leq y_g^s, \\ t_g(L), & \text{if } y_g^s < L. \end{cases}$$

## 4 Numerical scheme

The main advantage of dimension 1 is that equations in (1) are decoupled which means it suffices to compute  $h$  from equation (20) to deduce all other variables. To solve the transport equation with source term (20), the numerical method of characteristics (MOC) seems suitable insofar as it enables to cope with the advection operator.

Given  $\Delta y > 0$  and  $\Delta t > 0$ , we consider a uniform Cartesian grid  $\{y_i = i\Delta y\}_{1 \leq i \leq N}$  such that  $y_1 = 0$  and  $y_N = L$  (see Figure 6) as well as a time discretization  $\{t^n = n\Delta t\}_{n \geq 0}$ . Unknowns are collocated at the nodes of the mesh. We set the initial values  $v_i^0 = v_0(y_i)$  and  $h_i^0 = h_0(y_i)$  for  $i = 1, \dots, N$ .

### 4.1 Key idea of the scheme

For details about numerical methods of characteristics, the reader may refer to [17, 29]. This method amounts to tracking particles along the flow as it consists in building approximate characteristic curves to locate accurately the position of particles and updating the unknown according to the source term as described from a theoretical point of view in section 3.1. More precisely, at time  $t^n$ , we aim at approximating the solution of

$$\frac{d}{d\tau} \tilde{h}_i^{n+1}(\tau) = \frac{\beta(\tilde{h}_i^{n+1}(\tau)) \Phi(\tau, \chi(\tau; t^{n+1}, y_i))}{p_0} \left( \tilde{h}_i^{n+1}(\tau) - q(\tilde{h}_i^{n+1}(\tau)) \right), \quad (31a)$$

where  $\tau \mapsto \tilde{h}_i^{n+1}(\tau) \stackrel{\text{def}}{=} h(\tau, \chi(\tau; t^{n+1}, y_i))$  and the characteristic flow  $\chi$  satisfies

$$\begin{cases} \frac{d}{d\tau} \chi(\tau; t^{n+1}, y_i) = v(\tau, \chi(\tau; t^{n+1}, y_i)), & \tau \leq t^{n+1}, \\ \chi(t^{n+1}; t^{n+1}, y_i) = y_i. \end{cases} \quad (31b)$$

The reader may refer to [29] for further details about the resolution of (31b). Let  $\xi_i^n$  be the numerical approximation of  $\chi(t^n; t^{n+1}, y_i)$ . As for ODE (31a), any direct numerical method (except the explicit 1st-order Euler method) involves computations of the enthalpy at intermediate

times in  $(t^n, t^{n+1}]$ . The classical Euler-type MOC method is thus written as

$$h(t^{n+1}, y_i) = \tilde{h}_i^{n+1}(t^{n+1}) \approx \tilde{h}_i^{n+1}(t^n) + \Delta t \frac{\beta(\tilde{h}_i^{n+1}(t^n)) \Phi(\tau, \xi_i^n)}{p_0} \left( \tilde{h}_i^{n+1}(t^n) - q(\tilde{h}_i^{n+1}(t^n)) \right). \quad (32)$$

The difficulty lies in interpolating the numerical solution at time  $t^n$  (and located at nodes  $y_j$ ) to compute  $\tilde{h}_i^{n+1}(t^n) = h(t^n, \chi(t^n; t^{n+1}, y_i))$ . This step will be detailed later on. Scheme (32) will be referred to as the MOC scheme in the sequel.

To reach higher order, we rewrite ODE (31a) using the facts that  $\beta(h)$  and  $h - q(h)$  are positive. Setting

$$R(\tilde{h}) \stackrel{\text{def}}{=} \int_0^{\tilde{h}} \frac{dh}{\beta(h) \cdot (h - q(h))},$$

equation (31a) reads

$$R'(\tilde{h}_i^{n+1}) \frac{d}{d\tau} \tilde{h}_i^{n+1}(\tau) = \frac{\Phi(\tau, \chi(\tau; t^{n+1}, y_i))}{p_0} \quad (33)$$

and thus can be integrated explicitly between  $t^n$  and  $t^{n+1}$

$$R(\tilde{h}_i^{n+1}(t^{n+1})) - R(\tilde{h}_i^{n+1}(t^n)) = \frac{1}{p_0} \int_{t^n}^{t^{n+1}} \Phi(\tau, \chi(\tau; t^{n+1}, y_i)) d\tau$$

so that

$$\tilde{h}_i^{n+1}(t^{n+1}) = R^{-1} \left( R(\tilde{h}_i^{n+1}(t^n)) + \frac{1}{p_0} \int_{t^n}^{t^{n+1}} \Phi(\tau, \chi(\tau; t^{n+1}, y_i)) d\tau \right). \quad (34)$$

As  $\Phi$  is a datum, the right hand side can be expanded at any order. Notice that we can give explicit expressions for  $R$  and  $R^{-1}$ :

$$R(h) = \begin{cases} \frac{1}{\beta_\ell} \ln \left( 1 - \frac{h}{q_\ell} \right), & \text{if } h \leq h_\ell^s, \\ R_\ell^s + \frac{1}{\beta_m} \ln \left( \frac{h - q_m}{h_\ell^s - q_m} \right), & \text{if } h_\ell^s < h < h_g^s, \\ R_g^s + \frac{1}{\beta_g} \ln \left( \frac{h - q_g}{h_g^s - q_g} \right), & \text{if } h \geq h_g^s, \end{cases}$$

$$R^{-1}(r) = \begin{cases} q_\ell - q_\ell e^{\beta_\ell r}, & \text{if } r \leq R_\ell^s, \\ q_m + (h_\ell^s - q_m) e^{\beta_m (r - R_\ell^s)}, & \text{if } R_\ell^s < r < R_g^s, \\ q_g + (h_g^s - q_g) e^{\beta_g (r - R_g^s)}, & \text{if } r \geq R_g^s, \end{cases}$$

where

$$R_\ell^s \stackrel{\text{def}}{=} \frac{1}{\beta_\ell} \ln \left( 1 - \frac{h_\ell^s}{q_\ell} \right), \quad R_g^s \stackrel{\text{def}}{=} R_\ell^s + \frac{1}{\beta_m} \ln \left( \frac{h_g^s - q_m}{h_\ell^s - q_m} \right).$$

Strategy (34) intrinsically ensures the positivity of  $h_i^{n+1} - q(h_i^{n+1})$  and is named INTMOC.

## 4.2 Description of the scheme

Given the numerical solutions  $(h_i^n, v_i^n, \bar{p}_i^n)$ , the overall process at step  $n + 1$  consists in computing successively  $h_i^{n+1}$ ,  $v_i^{n+1}$  and  $\bar{p}_i^{n+1}$  as follows.

- ENTHALPY. For the boundary condition ( $i = 1$ ) we impose  $h_1^{n+1} = h_e(t^{n+1})$ . Then  $h_i^{n+1}$  is determined in two steps:

① Solve ODE (31b) over the interval  $[t^n, t^{n+1}]$ . The approximation  $\xi_i^n$  of  $\chi(t^n; t^{n+1}, y_i)$  is computed either at order 1 or 2 (see [27–29] for more details):

(i) at order 1 in time, we have  $\chi(t^n; t^{n+1}, y_i) \approx y_i - \Delta t \cdot v(t^n, y_i)$  so that we set

$$\xi_i^n = y_i - \Delta t \cdot v_i^n;$$

(ii) at order 2 in time, we have

$$\chi(t^n; t^{n+1}, y_i) \approx y_i - \Delta t \cdot v(t^n, y_i) - \frac{1}{2} \Delta t^2 (\partial_t v(t^n, y_i) - v(t^n, y_i) \partial_y v(t^n, y_i))$$

so that we set

$$\xi_i^n = y_i - \Delta t \left( \frac{3}{2} v_i^n - \frac{1}{2} v_i^{n-1} \right) + \frac{\Delta t^2}{2} \frac{\beta(h_i^n)}{p_0} v_i^n \Phi(t^n, y_i).$$

② Update the enthalpy:

- if  $\xi_i^n > 0$  (see Figure 7a), let  $j$  be the index such that  $\xi_i^n \in [y_j, y_{j+1})$ . Let us denote  $\theta_{ij}^n \stackrel{\text{def}}{=} \frac{y_{j+1} - \xi_i^n}{\Delta x}$  and  $\hat{h}_i^n$  the numerical approximation of  $h(t^n, \xi_i^n)$  (which approaches  $\tilde{h}_i^{n+1}(t^n)$ ) obtained by interpolation ( $\xi_i^n$  is generally not a mesh node):

(i) at order 1

$$\hat{h}_i^n = \theta_{ij}^n h_j^n + (1 - \theta_{ij}^n) h_{j+1}^n; \quad (35)$$

(ii) at higher order

$$\hat{h}_i^n = \lambda_i^n h_j^- + (1 - \lambda_i^n) h_j^+ \quad (36)$$

where

$$\lambda_i^n \stackrel{\text{def}}{=} \begin{cases} \frac{1 + \theta_{ij}^n}{3}, & \text{if } \mathcal{P}_j^+(\theta_{ij}^n) \geq 0 \text{ and } \mathcal{P}_j^-(\theta_{ij}^n) \geq 0, \\ 0, & \text{if } \mathcal{P}_j^+(\theta_{ij}^n) \geq 0 \text{ and } \mathcal{P}_j^-(\theta_{ij}^n) < 0, \\ 1, & \text{if } \mathcal{P}_j^+(\theta_{ij}^n) < 0 \text{ and } \mathcal{P}_j^-(\theta_{ij}^n) \geq 0, \\ \theta_{ij}^n, & \text{otherwise,} \end{cases}$$

$$h_j^- \stackrel{\text{def}}{=} \begin{cases} h_j^n, & \text{if } \mathcal{P}_j^+(\theta_{ij}^n) < 0 \text{ and } \mathcal{P}_j^-(\theta_{ij}^n) < 0, \\ \frac{(\theta_{ij}^n)^2}{2} (h_{j-1}^n - 2h_j^n + h_{j+1}^n) - \frac{\theta_{ij}^n}{2} (h_{j-1}^n - 4h_j^n + 3h_{j+1}^n) + h_{j+1}^n, & \text{otherwise,} \end{cases}$$

$$h_j^+ \stackrel{\text{def}}{=} \begin{cases} h_{j+1}^n, & \text{if } \mathcal{P}_j^+(\theta_{ij}^n) < 0 \text{ and } \mathcal{P}_j^-(\theta_{ij}^n) < 0, \\ \frac{(\theta_{ij}^n)^2}{2} (h_{j+2}^n - 2h_{j+1}^n + h_j^n) - \frac{\theta_{ij}^n}{2} (h_{j+2}^n - h_j^n) + h_{j+1}^n, & \text{otherwise,} \end{cases}$$

and  $\mathcal{P}_j^\pm(\theta) \stackrel{\text{def}}{=} (\theta - \delta_j^\pm)(\theta - \delta_{j+1}^\pm)$  with

$$\delta_j^- \stackrel{\text{def}}{=} \frac{2(h_{j+1}^n - h_j^n)}{h_{j-1}^n - 2h_j^n + h_{j+1}^n}, \quad \delta_j^+ \stackrel{\text{def}}{=} \frac{2(h_{j+1}^n - h_j^n)}{h_j^n - 2h_{j+1}^n + h_{j+2}^n},$$

$$\delta_{j+1}^- \stackrel{\text{def}}{=} \frac{h_{j-1}^n - 4h_j^n + 3h_{j+1}^n}{h_{j-1}^n - 2h_j^n + h_{j+1}^n}, \quad \delta_{j+1}^+ \stackrel{\text{def}}{=} \frac{h_{j+2}^n - h_j^n}{h_j^n - 2h_{j+1}^n + h_{j+2}^n}.$$

This procedure has been designed in [29] in order to ensure the maximum principle by means of a variable stencil. Even if there is no maximum principle associated to equation (20), this scheme preserves the property  $\hat{h}_i^n - q(\hat{h}_i^n) > 0$ .

We then update  $h_i^{n+1}$  by formulae (32) or (34):

- (i) if we use the standard MOC scheme for ODE (31a) over  $[t^n, t^{n+1}]$ , (32) reads

$$h_i^{n+1} = \hat{h}_i^n + \Delta t \frac{\beta(\hat{h}_i^n) \Phi(t^n, \xi_i^n)}{p_0} (\hat{h}_i^n - q(\hat{h}_i^n)); \quad (37a)$$

- (ii) if we modify equation (31a) before integration, the trapezoidal formula applied to the right hand side in (34) yields

$$h_i^{n+1} = R^{-1} \left( R(\hat{h}_i^n) + \frac{\Delta t}{p_0} \frac{\Phi(t^n, \xi_i^n) + \Phi(t^{n+1}, y_i)}{2} \right); \quad (37b)$$

- if  $\xi_i^n \leq 0$  (see Figure 7b), we compute the time  $t_i^*$  at which the characteristic curve  $\tau \mapsto \chi(\tau; t^{n+1}, y_i)$  crosses the inflow boundary. There we have  $h(t_i^*, 0) = h_e(t_i^*)$ . Using a first order approximation in time, we set  $t_i^* = t^{n+1} - y_i/v_i^n$  and we compute the updated enthalpy similarly to what is detailed above:

- (i) by integrating ODE (31a) over  $[t_i^*, t^{n+1}]$  (Euler scheme in time)

$$h_i^{n+1} = h_e(t_i^*) + (t^{n+1} - t_i^*) \frac{\beta(h_e(t_i^*)) \Phi(t_i^*, 0)}{p_0} [h_e(t_i^*) - q(h_e(t_i^*))]; \quad (38a)$$

- (ii) by integrating ODE (33) over  $[t_i^*, t^{n+1}]$  (trapezoidal formula)

$$h_i^{n+1} = R^{-1} \left( R(h_e(t_i^*)) + \frac{t^{n+1} - t_i^*}{p_0} \frac{\Phi(t_i^*, 0) + \Phi(t^{n+1}, y_i)}{2} \right). \quad (38b)$$

The boundary  $y = 0$  is the only one we need to care about since characteristic curves cannot exit from the domain at  $y = L$  (we assumed that  $v_e > 0$  and  $\Phi \geq 0$  which implies that  $v > 0$ ).

- VELOCITY. For the boundary condition ( $i = 1$ ), we set  $v_1^{n+1} = v_e(t^{n+1})$ . Then, we integrate equation (1a) over  $[y_i, y_{i+1}]$ . Depending on the ability to compute the primitive function of  $\Phi$ , the velocity field can be computed directly

$$v_i^{n+1} = v_{i-1}^{n+1} + \frac{1}{p_0} \int_{y_{i-1}}^{y_i} \beta(h(t^{n+1}, z)) \Phi(t^{n+1}, z) dz, \quad \text{for } i = 2, \dots, N$$

or approximated by the following upwind approach (since  $v_i^n \geq 0$  for all  $i$  and for all  $n$ )

$$v_i^{n+1} = v_{i-1}^{n+1} + \frac{\Delta y}{p_0} \beta(h_{i-1}^{n+1}) \Phi(t^{n+1}, y_{i-1}).$$

However, since the coefficient  $\beta$  is discontinuous at phase change points (see Figure 3c), we have to adapt the previous algorithm in cells where the fluid changes from a phase to

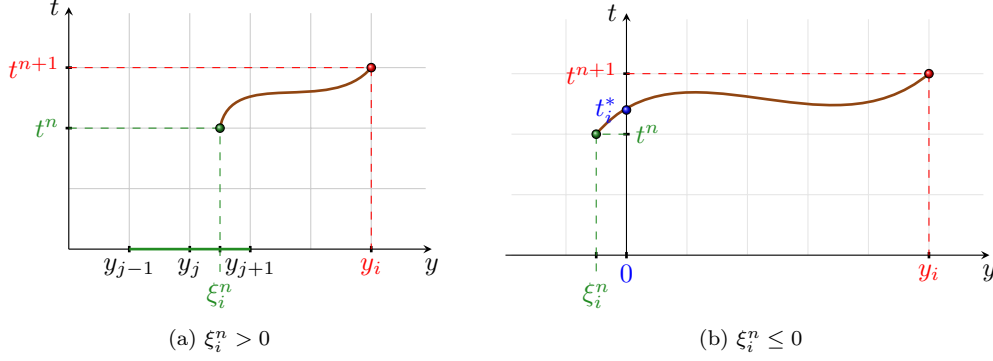


Figure 7: Numerical method of characteristics.

another. It is reasonable to suppose that at most two phases are present within a single cell. Then, if  $h_\kappa^s \in (h_{i-1}^{n+1}, h_i^{n+1})$ , let  $y^*$  be the linear approximation of  $y_\kappa^s$ , *i.e.*

$$y^* \stackrel{\text{def}}{=} y_{i-1} + \Delta y \frac{h_\kappa^s - h_{i-1}^{n+1}}{h_i^{n+1} - h_{i-1}^{n+1}}.$$

Hence

$$\begin{aligned} & \int_{y_{i-1}}^{y_i} \beta(h(t^{n+1}, z)) \Phi(t^{n+1}, z) dz \\ &= \int_{y_{i-1}}^{y^*} \beta(h(t^{n+1}, z)) \Phi(t^{n+1}, z) dz + \int_{y^*}^{y_i} \beta(h(t^{n+1}, z)) \Phi(t^{n+1}, z) dz \\ &\approx (y^* - y_{i-1}) \beta(h_{i-1}^{n+1}) \Phi(t^{n+1}, y_{i-1}) + (y_i - y^*) \beta(h_i^{n+1}) \Phi(t^{n+1}, y_i). \end{aligned}$$

- **PRESSURE.** For the boundary condition ( $i = N$ ), we set  $\bar{p}_N^n = p_0$ . Then we rewrite equation (1c) in the following equivalent form

$$\begin{aligned} -\partial_y \bar{p} &= \partial_t (\rho(h)v) + \partial_y (\rho(h)v^2) - \partial_y (\mu \partial_y v) + \rho(h)g \\ &= \rho(h) \partial_t v + \rho(h)v \partial_y v - \partial_y (\mu \partial_y v) + \rho(h)g. \end{aligned}$$

Using (1a) it becomes

$$-\partial_y \bar{p} = \rho(h) \partial_t v + \rho(h)v \frac{\beta(h)\Phi}{p_0} - \partial_y \left( \mu \frac{\beta(h)\Phi}{p_0} \right) + \rho(h)g.$$

Let us note  $\rho_i^{n+1} = \rho(h_i^{n+1})$  and  $\beta_i^{n+1} = \beta(h_i^{n+1})$ . Integrating this equation over  $[y_{i-1}, y_i]$ , we obtain

$$\begin{aligned} \bar{p}_{i-1}^{n+1} &= \bar{p}_i^{n+1} + \frac{\Delta y}{2} \left[ (\rho_i^{n+1} + \rho_{i-1}^{n+1})g + \rho_i^{n+1} \frac{v_i^{n+1} - v_i^n}{\Delta t} + \rho_{i-1}^{n+1} \frac{v_{i-1}^{n+1} - v_{i-1}^n}{\Delta t} \right. \\ &\quad \left. + \rho_i^{n+1} v_i^{n+1} \frac{\beta_i^{n+1}}{p_0} \Phi(t^{n+1}, y_i) + \rho_{i-1}^{n+1} v_{i-1}^{n+1} \frac{\beta_{i-1}^{n+1}}{p_0} \Phi(t^{n+1}, y_{i-1}) \right] \\ &\quad - \mu \left[ \frac{\beta_i^{n+1}}{p_0} \Phi(t^{n+1}, y_i) - \frac{\beta_{i-1}^{n+1}}{p_0} \Phi(t^{n+1}, y_{i-1}) \right], \quad i \in \{2, \dots, N\}. \end{aligned} \tag{39}$$

Both schemes (MOC and INTMOC) are explicit and unconditionally stable which are standard features for numerical methods of characteristics. The handling of boundary conditions is achieved in the present study at order 1. Although the time step can be chosen independently from the mesh size, it must be small enough to provide accurate results.

## 5 Numerical examples

In this section we focus on data sets for which phase transition occurs (for the simulations of single-phase flows, we refer to [3]). To simulate some scenarii in a PWR, parameters are set as follows:

- Geometry of the reactor:  $L = 4.2$  m.
- Discretization parameters:  $N = 100$  mesh nodes ( $\Delta y \approx 4.3$  cm) and  $\Delta t = 0.01$  s.
- Parameters involved in EOS: *cf.* Table 1 at page 40.
- Reference value for the pressure, the power density and the velocity:  $p_0 = 155 \times 10^5$  Pa,  $\Phi_0 = 170 \times 10^6$  W  $\cdot$  m $^{-3}$ ,  $\tilde{v} = 0.5$  m  $\cdot$  s $^{-1}$ .
- Initial data:  $h_0(y) = h_e$ ,  $v_0(y) = v_e + \int_0^y \beta(h_0(z))\Phi(0, z)/p_0 dz$  (well-prepared insofar as they satisfy the divergence constraint (1a)).
- Constant viscosity:  $\mu_0 = 8.4 \cdot 10^{-5}$  kg  $\cdot$  m $^{-1}$   $\cdot$  s $^{-1}$ .

In Test 5.1 a two-phase flow with phase transition is considered and enables to compare the numerical schemes presented in section 4, while all other tests only involve scheme (37b)&(38b) with high order interpolation (36) (noted INTMOC\_2) to assess the robustness of the scheme and the relevance of the model.

### 5.1 Two-phase flow with phase transition

In the first test, we investigate the ability of our model to deal with two-phase flows with phase transition. We consider the case when the inlet density  $\rho_e$ , the inlet velocity  $v_e$ , the initial condition  $h_0$  and the power density  $\Phi$  are constant, so that we can apply Proposition 6 to compute exact transient and asymptotic solutions. The boundary conditions are  $\rho_e(t) = 750$  kg  $\cdot$  m $^{-3}$  and  $v_e(t) = \tilde{v}$ , thus  $h_0(y) = h_e(t) = h_\ell(\rho_e) \approx 1.190 \times 10^6$  J  $\cdot$  K $^{-1}$ . The power density is set constant in space and time and equal to  $\Phi_0$ . With these parameters, the domain is initially filled with liquid. Then at time  $t = 1.769$  s mixture appears for  $y > y_\ell^s \simeq 0.964$  m and at time  $t = 2.929$  s pure vapor appears for  $y > y_g^s \simeq 4.002$  m. The asymptotic state is reached at  $t = 2.957$  s.

Figure 8 displays numerical results for the enthalpy and the velocity at instants  $t = 2.1$  s,  $t = 2.8$  s and  $t = 3.5$  s. At this last time the solution has already reached the asymptotic regime. Figure 9 displays the mass fraction and the Mach number computed from the enthalpy and the velocity. Figure 10 displays the density and the temperature computed from the enthalpy.

In those figures we compare the exact and asymptotic solutions to the different versions of the numerical scheme, namely:

- by scheme (37a)&(38a) with linear interpolation (35) (called MOC\_1),

- by scheme (37a)&(38a) with high order interpolation (36) (called MOC\_2),
- by scheme (37b)&(38b) with linear interpolation (35) (called INTMOC\_1),
- by scheme (37b)&(38b) with high order interpolation (36) (called INTMOC\_2).

We observe that all numerical results match the behaviour of the exact solution including phase transition. Nevertheless as it can be noticed at time  $t = 2.8$  s, there is some discrepancy close to the singularity (interface between information coming from the boundary and the inner domain). This can easily be accounted for. Indeed, the scheme relies on an interpolation process which assumes some smoothness for the solution. As it is not smooth at the singularity, the scheme provides a smoothed version of the exact solution. It must be underlined that the higher the degree of interpolation, the most accurate the solution. Moreover, there is a clear advantage of INTMOC versions of the scheme over MOC which is due to the better approximation of the right hand side in the former case. For these reasons, from now on we will use only the INTMOC\_2 scheme which is more accurate.

Figure 9 shows that the Mach number remains lower than 0.05 so that the low Mach number hypothesis of the model is valid in this configuration. Observe that during the transient state, the Mach number is greater than at the asymptotic state.

From a physical point of view, it is worth emphasizing that our model predicts the appearance of some vapor at the top of the reactor for this data set. This is due to a too small inflow velocity.

## 5.2 Non monotone $\Phi$

We perform a simulation for a steady power density piecewise constant in space

$$\Phi(t, y) = \begin{cases} \Phi_0, & \text{if } y \leq L/2, \\ 0, & \text{if } y > L/2. \end{cases}$$

This power density models the situation where the control rods are blocked at the middle of the reactor. The boundary conditions are  $\rho_e(t) = 750 \text{ kg} \cdot \text{m}^{-3}$  and  $v_e(t) = \tilde{v}$ , thus  $h_0(y) = h_e(t) = h_\ell(\rho_e) \approx 1.190 \times 10^6 \text{ J} \cdot \text{K}^{-1}$ .

We plot on Figure 11 the asymptotic solution and the numerical one computed by means of the INTMOC\_2 scheme for the enthalpy, the mass fraction, the dynamical pressure, the density and the temperature at the instants  $t = 0.0$  s,  $t = 1.0$  s,  $t = 2.0$  s,  $t = 3.0$  s and  $t = 4.0$  s. The velocity is given at instants  $t < t_\ell^s$ ,  $t = 1.8$  s and  $t = 2.0$  s. The enthalpy evolves according to Proposition 6 and is continuous: over  $[0, L/2]$  it is linearly monotone-increasing and over  $[L/2, L]$  it evolves in time until the constant asymptotic state is reached. At the initial state the core is filled with liquid, so that the void fraction is 0. At  $t = t_\ell^s \simeq 1.768$  s mixture appears over  $[y_\ell^s, L/2]$  where  $y_\ell^s \simeq 0.964$  m. This mixture is transported to fill the domain  $y \geq y_\ell^s$ . As long as the domain is filled with liquid, the velocity does not depend on time. When mixture appears,  $\beta$  is piecewise constant in the domain so that, according to Proposition 6, the velocity increases up to the asymptotic value. The dynamical pressure is computed by scheme (39) and decreases until the asymptotic state.

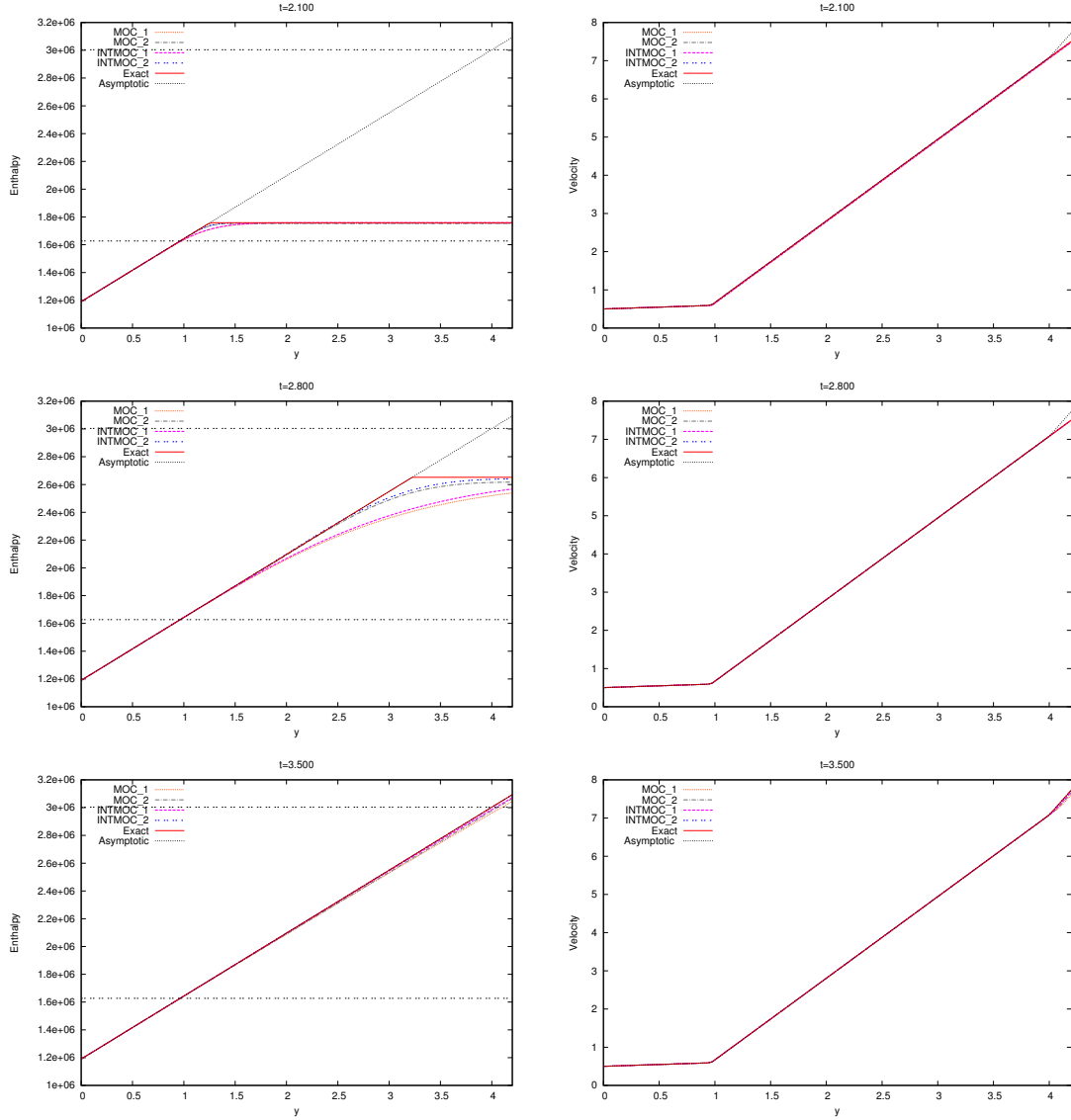


Figure 8: Numerical enthalpy (left) and velocity (right) for test 5.1: Two-phase flow with phase transition. We compare the four numerical solutions to the analytical and asymptotic ones. The horizontal dotted lines correspond to  $h = h_l^s$  and  $h = h_g^s$ .

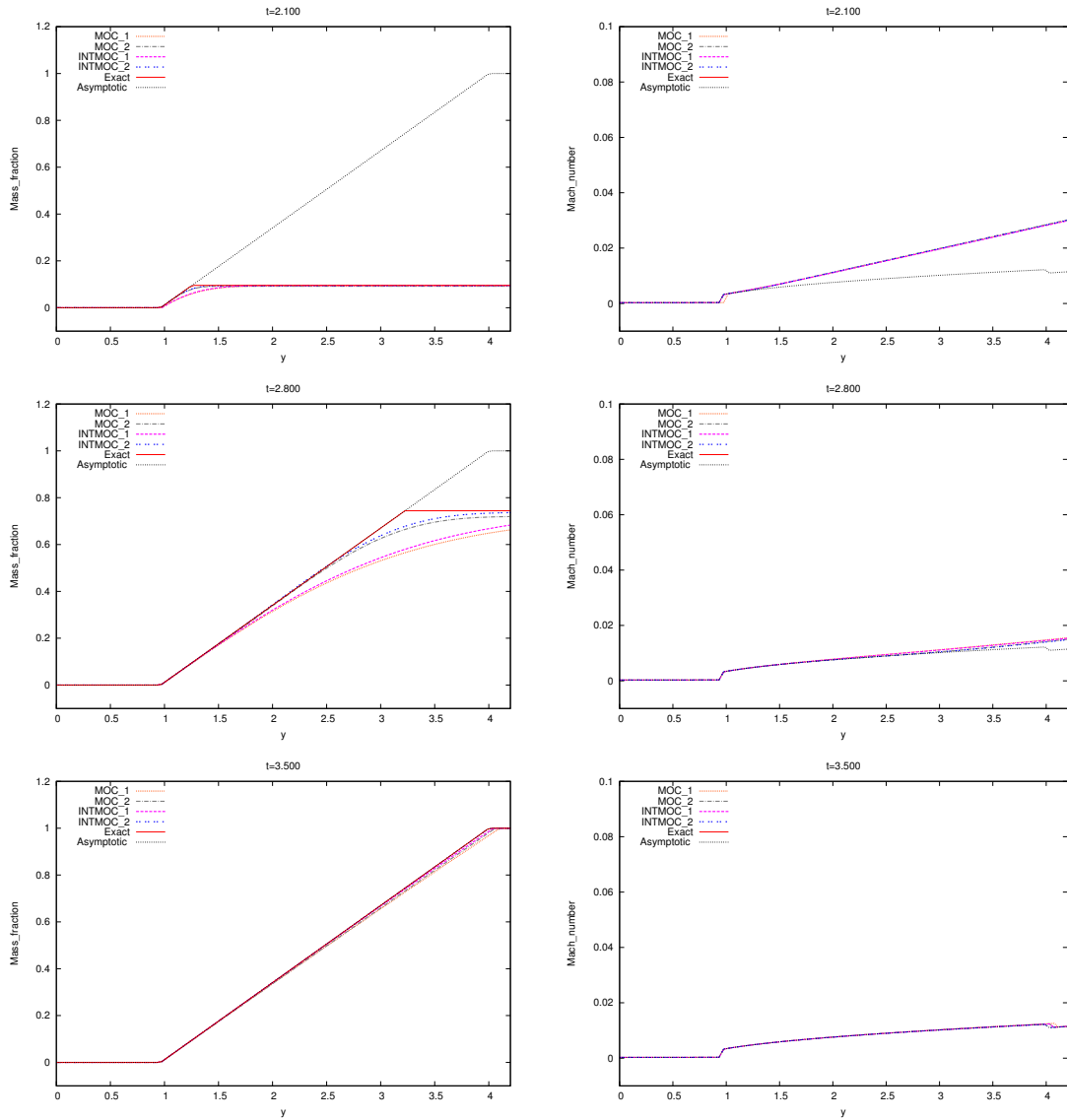


Figure 9: Numerical mass fraction (left) and speed of sound (right) of the test 5.1: Two-phase flow with phase transition. We compare the four numerical solutions with the analytical and asymptotic ones.

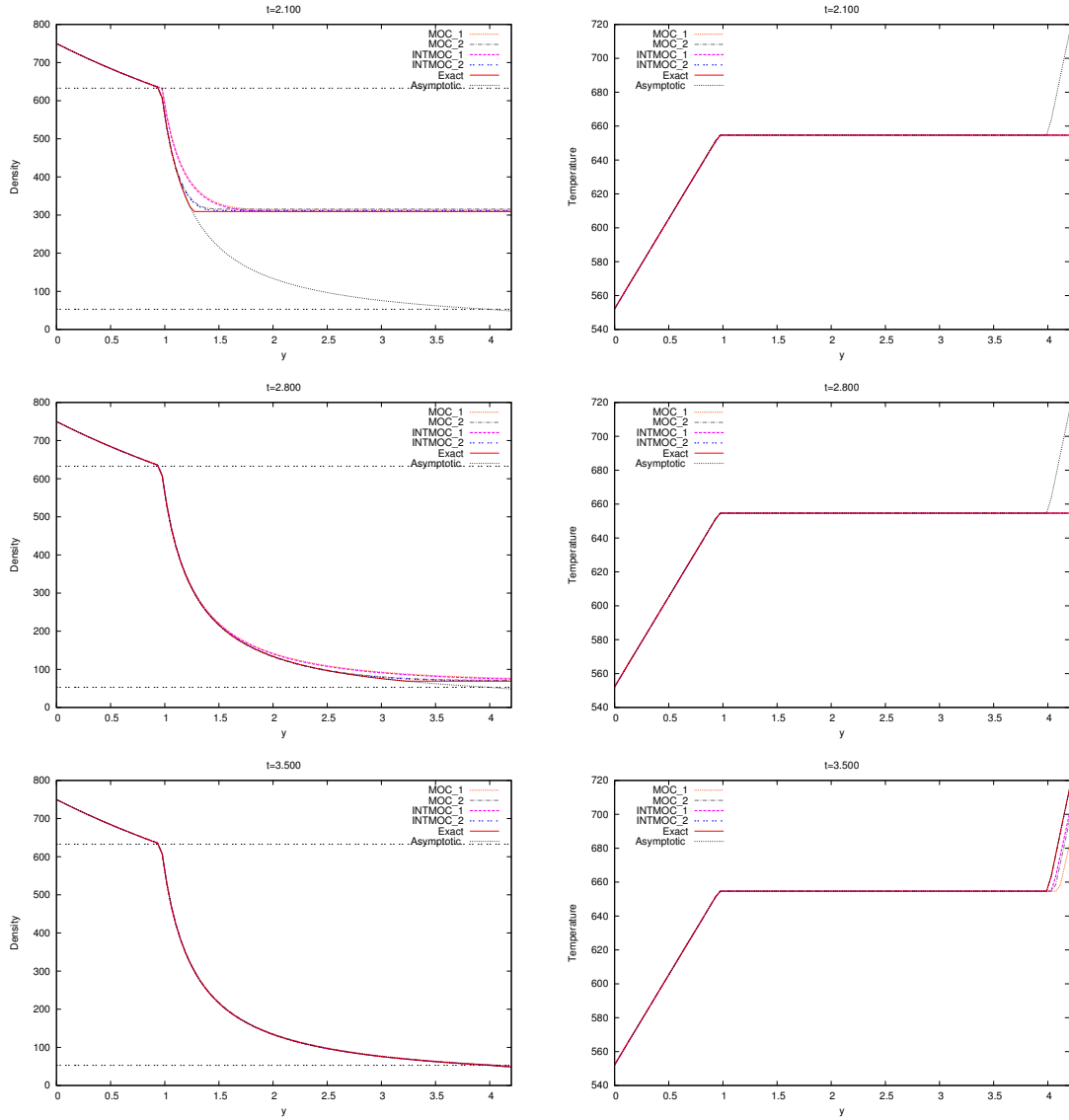
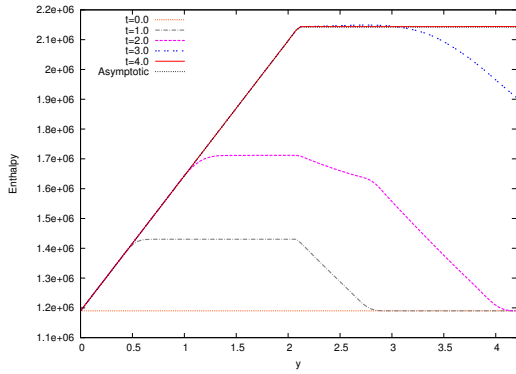
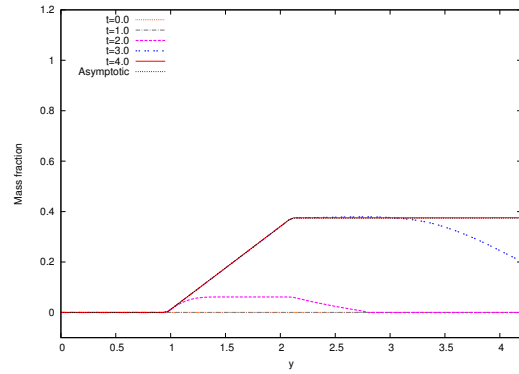


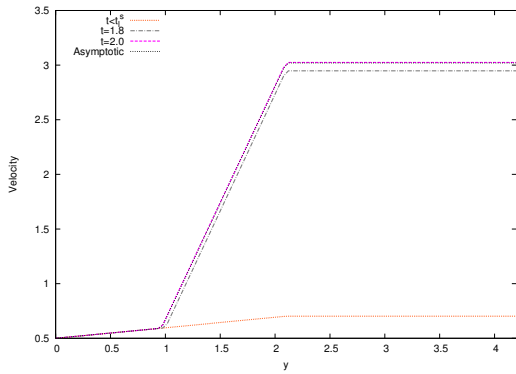
Figure 10: Numerical density (left) and temperature (right) of the test 5.1: Two-phase flow with phase transition. We compare the four numerical solutions with the analytical and asymptotic ones. The horizontal dotted lines correspond to  $\rho = \rho_l^s$  and  $\rho = \rho_g^s$ .



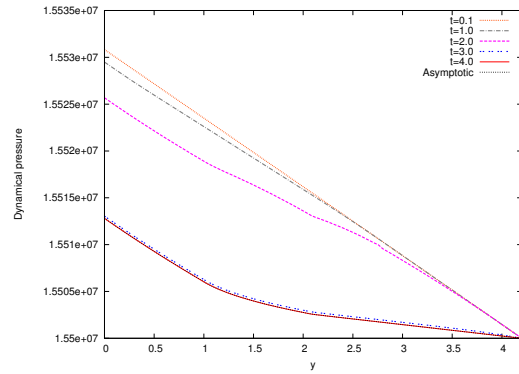
(a) Enthalpy



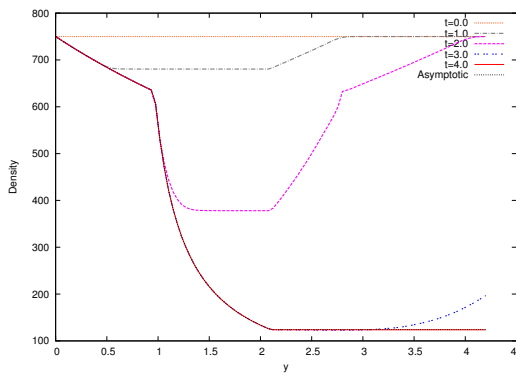
(b) Mass fraction



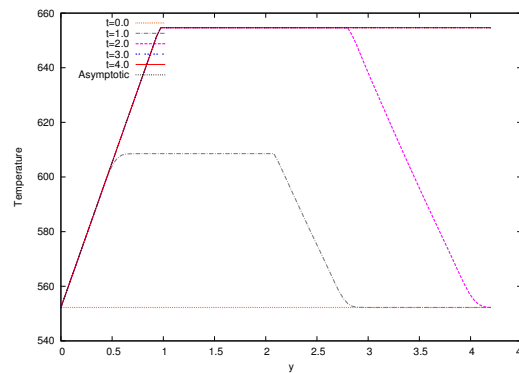
(c) Velocity



(d) Dynamical pressure



(e) Density



(f) Temperature

Figure 11: Numerical results of the test 5.2: Non monotone  $\Phi$ .

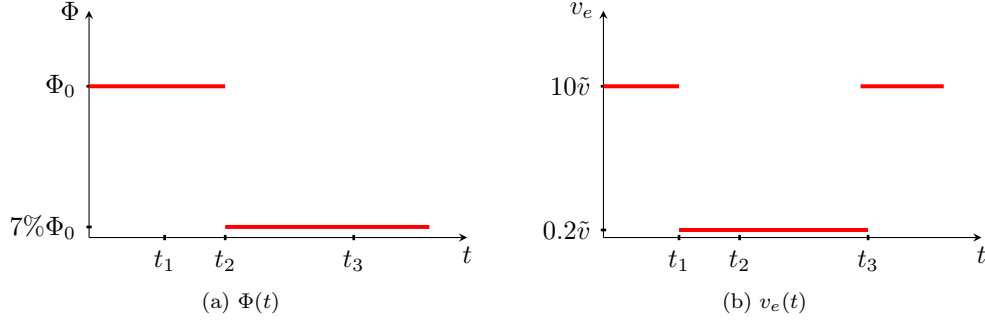


Figure 12: Power density and entrance velocity for the test 5.3: A simplified scenario for a Loss of Flow Accident.

### 5.3 A simplified scenario for a Loss of Flow Accident

Our model is tested here on an accidental transient regime: a main coolant pump trip which is a Loss Of Flow Accident (LOFA) as at the beginning of the Fukushima accident in reactors 1, 2 and 3. To simulate this scenario, the domain is filled at first with liquid water and we have a normal behaviour of the reactor: the pumps work normally and control rods are in upper position. We impose at the entrance the velocity  $v_e = 10\tilde{v}$  and the power density is equal to  $\Phi_0$ . These constants are chosen so as to prevent the appearance of mixture. The asymptotic state is reached at  $t \simeq 0.8$  s.

At time  $t_1 = 1.5$  s most of the pumps stop, so that the entrance velocity decreases. At time  $t_2$  the security system makes control rods drop into the core decreasing abruptly the power density. However, there is still some residual power density (about  $7\%\Phi_0$ ). This instant  $t_2 \simeq 2.85$  s corresponds to the moment of first appearance of mixture ( $t \simeq 2.55$  s) plus some time for the rods to be dropped (0.3 s). At time  $t_3$  the security pumps are turned on, thus the inflow is re-established. We then compute the solution until the asymptotic state is reached. Functions  $v_e(t)$  and  $\Phi(t)$  can be modelled as follows (see Figure 12):

$$v_e(t) = \begin{cases} 10\tilde{v} & \text{if } 0 \leq t < t_1, \\ 0.2\tilde{v} & \text{if } t_1 \leq t < t_3, \\ 10\tilde{v} & \text{if } t \geq t_3, \end{cases} \quad \Phi(t) = \begin{cases} \Phi_0 & \text{if } 0 \leq t < t_2, \\ 7\%\Phi_0 & \text{if } t \geq t_2. \end{cases}$$

In Figure 13 we report the behaviour of the mass fraction and temperature computed at different instants. Thanks to our model we can predict the appearance of some steam in the core depending of the value of  $t_3$ :

Case A: for  $t_3 = 40$  s the asymptotic state corresponding to  $\Phi = 7\%\Phi_0$  and  $v_e = 0.2\tilde{v}$  is established. In this case, due to the residual power density the fluid is completely vaporized at the top of the domain during the transition (see for example Figure 13a at time  $t = 30$  s) even though there are only liquid and mixture phases in the corresponding asymptotic state.

Case B: for  $t_3 = 20$  s the pumps are re-started soon enough so that the appearance of pure steam is avoided.

Case C: for  $t_3 = 4$  s, even though the pumps are re-started almost instantaneously, some mixture appears in a large part of the domain.

In all cases, when the pumps are re-started the fluid comes back to the liquid phase. As expected, the sooner the pumps are re-started, the safer the situation.

## 6 Conclusion & Perspectives

We proposed in this paper simulations of a low Mach number model – named LMNC – for fluid flows in nuclear reactor cores coupled to an adaptive stiffened gas equation of state (EOS) which varies according to the phase of the coolant fluid (which can be pure liquid water, pure steam or mixture of these two phases). The monodimensional (1D) numerical strategy we worked out lead to accurate and relevant qualitative results in accordance with what was expected. These results were obtained with an optimal computational cost since the velocity and the dynamic pressure are directly integrated in the 1D case.

More precisely, compared to a previous study [3], the present work enables to deal with more realistic situations insofar as the model allows for phase transition and, thus, for accidental scenarii such as a Loss of Flow Accident (LOFA) induced by a coolant pump trip event. Nevertheless, the method used to determine parameters involved in the stiffened gas EOS seems to be restrictive given the range of temperature that must be considered. That is why another strategy will be investigated in [14] using tabulated laws instead of the stiffened gas EOS.

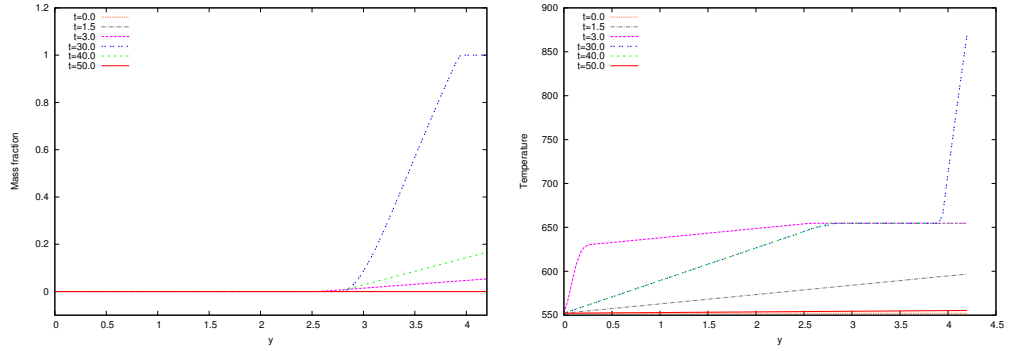
From a numerical point of view, a variant of the classical method of characteristics was proposed. It relies on the EOS and provided second-order accurate results. This algorithm was compared to the unsteady analytical solutions derived in this study for different data sets including configurations where phase transition occurs.

Moreover, we recall that the thermodynamic pressure is constant in the LMNC model. Hence, whatever the EOS used to model each phase and no matter what the dimension of the domain (1D, 2D or 3D), the computational cost related to the EOS will be much lower in the discretization of the LMNC model than in any strategy for the compressible model.

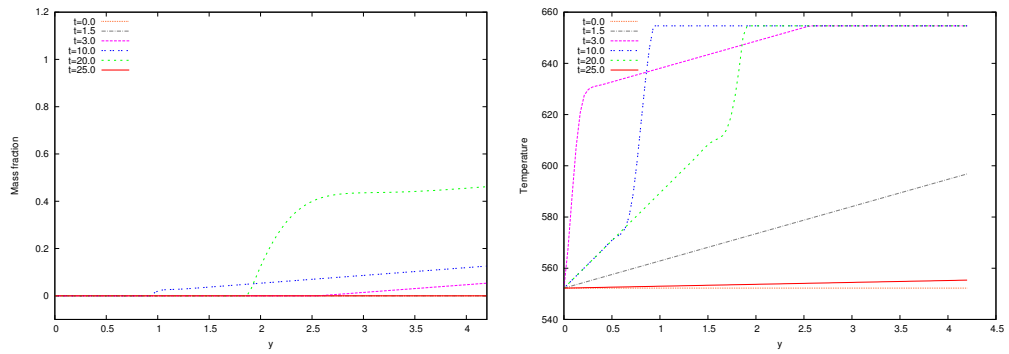
The adaptation of the proposed algorithm to dimensions 2 and 3 will be carried out in future works as well as the study of finite-volume based algorithms such as the method detailed in [5] which must be modified to match the low Mach number regime. However, it must be underlined that although the LMNC model may be a useful tool for safety studies, it is not designed to handle all potential situations especially when the Mach number cannot be considered as small anymore. This is why it is important to study the possibility to couple the LMNC model to the compressible system from which it is derived [13]. Likewise, couplings with systems dedicated to other circuits in the reactor must be contemplated.

## Appendix

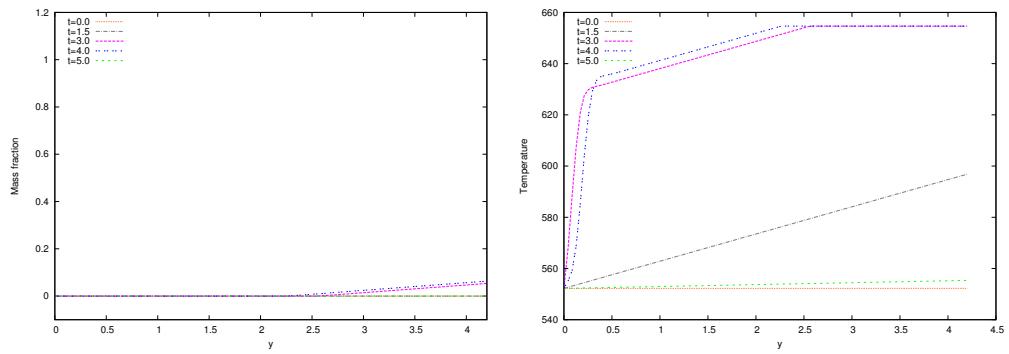
In this appendix, we follow the method introduced in [23, 24] to choose parameters describing each pure phase of water with a stiffened gas law to fit with saturated curves (see Figure 2a). Then, we determine relevant values for liquid water and steam.



(a) Case A



(b) Case B



(c) Case C

Figure 13: Numerical mass fraction (left) and temperature (right) of the test 5.3: A simplified scenario for a Loss of Flow Accident.

More precisely, we suppose that each phase is described by its own stiffened gas EOS (18), so that we have to compute five constants for each phase: the specific heat at constant volume  $c_{v,\kappa}$ , the adiabatic coefficient  $\gamma_\kappa$ , the reference pressure  $\pi_\kappa$ , the binding energy  $q_\kappa$  and the reference entropy  $q'_\kappa$  ( $\kappa = \ell$  refers to the liquid phase and  $\kappa = g$  to the vapor one). These parameters will be determined using experimental values at saturation.

The stiffened gas law consists of the following expressions for the density, the enthalpy and the Gibbs potential as functions of the temperature  $T$  and the pressure  $p$ :

$$\rho_\kappa(T, p) = \frac{p + \pi_\kappa}{(\gamma_\kappa - 1)c_{v,\kappa}T}, \quad (40a)$$

$$h_\kappa(T, p) = q_\kappa + \gamma_\kappa c_{v,\kappa}T, \quad (\text{independent of } p) \quad (40b)$$

$$g_\kappa(T, p) = q_\kappa + T(c_{v,\kappa}\gamma_\kappa - q'_\kappa - c_{v,\kappa}\gamma_\kappa \ln T + c_{v,\kappa}(\gamma_\kappa - 1) \ln(p + \pi_\kappa)), \quad (40c)$$

For a given temperature  $\bar{T}$ , the experimental data needed for the computation are the pressure at saturation  $p_{\text{exp}}^s(\bar{T})$ , the enthalpies at saturation  $h_{\kappa,\text{exp}}^s(\bar{T})$  and the densities at saturation  $\rho_{\kappa,\text{exp}}^s(\bar{T})$ . We can find these data in [25] for several fluids. Let  $T_0$  and  $T_1$  two reference temperatures (recorded in [25]) between the triple point and the critical point (see Figure 2b).

- STEP I: COMPUTATION OF  $\gamma_\kappa c_{v,\kappa}$ . From the analytical expression of the enthalpy (40b) we have  $h'_\kappa(T) = \gamma_\kappa c_{v,\kappa}$ . This yields an averaged value of the product  $c_{p,\kappa} \stackrel{\text{def}}{=} \gamma_\kappa c_{v,\kappa}$  by means of a linear approximation of the experimental enthalpies between reference states  $T_0$  and  $T_1$  as

$$c_{p,\kappa} = \frac{h_{\kappa,\text{exp}}^s(T_1) - h_{\kappa,\text{exp}}^s(T_0)}{T_1 - T_0}. \quad (41)$$

- STEP II: COMPUTATION OF  $q_\kappa$ . Equation (40b) applied to the reference state  $T_0$  provides the approximation of the binding energy  $q_\kappa$ :

$$q_\kappa = h_{\kappa,\text{exp}}^s(T_0) - c_{p,\kappa}T_0.$$

- STEP III: COMPUTATION OF  $\pi_\kappa$ . At saturation, there is an algebraic relation between the temperature and the pressure, *e.g.* we can write  $p = p^s(T)$ . Thus, using (40a), the specific densities at saturation are expressed as

$$\rho_\kappa^s(T) = \rho_\kappa(T, p^s(T)) = \frac{p^s(T) + \pi_\kappa}{(c_{p,\kappa} - c_{v,\kappa})T}, \quad (42)$$

which implies

$$\ln \rho_\kappa^s(T) = \ln(p^s(T) + \pi_\kappa) - \ln(c_{p,\kappa} - c_{v,\kappa}) - \ln T.$$

Evaluating this equation at  $T_0$  and  $T_1$  yields

$$\ln \left( \frac{\rho_\kappa^s(T_1)}{\rho_\kappa^s(T_0)} \right) = \ln \left( \frac{p^s(T_1) + \pi_\kappa}{p^s(T_0) + \pi_\kappa} \right) - \ln \left( \frac{T_1}{T_0} \right),$$

or equivalently

$$\frac{\rho_\kappa^s(T_1)}{\rho_\kappa^s(T_0)} = \frac{(p^s(T_1) + \pi_\kappa)T_0}{(p^s(T_0) + \pi_\kappa)T_1},$$

so that we can determine an averaged value of the coefficient  $\pi_\kappa$  using experimental values of the density and the pressure at saturation

$$\pi_\kappa = \frac{T_0 \rho_{\kappa,\text{exp}}^s(T_0) p_{\text{exp}}^s(T_1) - T_1 \rho_{\kappa,\text{exp}}^s(T_1) p_{\text{exp}}^s(T_0)}{T_1 \rho_{\kappa,\text{exp}}^s(T_1) - T_0 \rho_{\kappa,\text{exp}}^s(T_0)}.$$

Phase	$c_v$ [J · K <sup>-1</sup> ]	$\gamma$	$\pi$ [Pa]	$q$ [J · kg <sup>-1</sup> ]	$q'$ [J · K <sup>-1</sup> ]
Liquid	1816.2	2.35	10 <sup>9</sup>	$-1167.056 \times 10^3$	-0.0000028
Vapor	1040.14	1.43	0	$2030.255 \times 10^3$	-23310.00000

Table 1: Liquid water and steam, parameters computed in [23, 24].

- STEP IV: COMPUTATION OF  $c_{v_\kappa}$ . Equation (42) applied to the reference state  $T_0$  provides the approximation of  $c_{v_\kappa}$

$$c_{v_\kappa} = c_{p_\kappa} - \frac{p_{\text{exp}}^s(T_0) + \pi_\kappa}{T_0 \rho_{\kappa, \text{exp}}^s(T_0)}.$$

- STEP V: COMPUTATION OF  $\gamma_\kappa$ . Using (41) we deduce the approximation of  $\gamma_\kappa$

$$\gamma_\kappa = \frac{c_{p_\kappa}}{c_{v_\kappa}}.$$

- STEP VI: COMPUTATION OF  $q'_\kappa$ . At thermodynamic equilibrium, the two Gibbs potentials are equal. Using (40c), this implies

$$A \ln(p^s(T) + \pi_g) - B \ln(p^s(T) + \pi_\ell) - C(\ln T - 1) + \frac{D}{T} + q'_\ell - q'_g = 0$$

with

$$A \stackrel{\text{def}}{=} c_{p_g} - c_{v_g}, \quad B \stackrel{\text{def}}{=} c_{p_\ell} - c_{v_\ell}, \quad C \stackrel{\text{def}}{=} c_{p_g} - c_{p_\ell}, \quad D \stackrel{\text{def}}{=} q_g - q_\ell.$$

By convention, we take  $q'_\ell = 0 \text{ J} \cdot \text{K}^{-1}$  and determine the coefficient  $q'_g$  using experimental values of the pressure at saturation

$$q'_g = A \ln(p_{\text{exp}}^s(T_0) + \pi_g) - B \ln(p_{\text{exp}}^s(T_0) + \pi_\ell) - C(\ln T_0 - 1) + \frac{D}{T_0}.$$

Reference states  $T_0$  and  $T_1$  must now be specified. First,  $T_0$  is a reference state chosen in order to have the best fit between the theoretical pressure  $p^s(T)$  and the experimental one  $p_{\text{exp}}^s(T)$ . Secondly, this strategy for the determination of parameters for a stiffened gas EOS is accurate if the two reference states are sufficiently close. Practically (following [23, 24]), we took for the liquid phase  $T_0 = 298 \text{ K}$  and  $T_1 = 473 \text{ K}$  (steps I and II) and  $T_0 = 439 \text{ K}$  and  $T_1 = 588 \text{ K}$  (steps III to VI). As for the steam, we set  $T_0 = 298 \text{ K}$  and  $T_1 = 473 \text{ K}$  in any step.

The values for liquid water and steam are given in Table 1. These parameter values yield reasonable approximations over a temperature range from 298 K to 473 K.

Nevertheless near the critical point, there are some restrictions due to the nonlinearity of the enthalpy with respect to the temperature. To circumvent this limitation, we shall propose in [14] a new strategy to better approximate the thermodynamic quantities involved in the LMNC model.

## References

- [1] TRACE V5.0 Theory Manual, Field Equations, Solution Methods and Physical Models. Technical report, U.S. Nuclear Regulatory Commission, 2008.

- [2] G. Allaire, G. Faccanoni, and S. Kokh. A strictly hyperbolic equilibrium phase transition model. *C. R. Acad. Sci. Paris Sér. I*, 344:135–140, 2007.
- [3] M. Bernard, S. Dellacherie, G. Faccanoni, B. Grec, O. Lafitte, T.-T. Nguyen, and Y. Penel. Study of low Mach nuclear core model for single-phase flow. Accepted in ESAIM: Proc.
- [4] D. Bestion. The physical closure laws in the cathare code. *Nuclear Engineering and Design*, 124(3):229–245, 1990.
- [5] C. Calgaro, E. Creusé, and T. Goudon. An hybrid finite volume-finite element method for variable density incompressible flows. *J. Comput. Phys.*, 227(9):4671–4696, 2008.
- [6] H. B. Callen. *Thermodynamics and an Introduction to Thermostatistics*. John Wiley & sons, second edition, 1985.
- [7] S. Clerc. Numerical Simulation of the Homogeneous Equilibrium Model for Two-Phase Flows. *Journal of Computational Physics*, 181(2):577–616, 2002.
- [8] J.M. Delhayé. *Thermohydraulique des réacteurs*. EDP sciences, 2008.
- [9] S. Dellacherie. On a diphasic low Mach number system. *Math. Model. and Num. Anal.*, 39, 2005.
- [10] S. Dellacherie. Numerical resolution of a potential diphasic low Mach number system. *Journal of Computational Physics*, 223(1):151–187, 2007.
- [11] S. Dellacherie. Analysis of Godunov type schemes applied to the compressible Euler system at low Mach number. *Journal of Computational Physics*, 229(4):978–1016, 2010.
- [12] S. Dellacherie. On a low Mach nuclear core model. *ESAIM: Proc*, 35:79–106, 2012.
- [13] S. Dellacherie, B. Després, and Y. Penel. A first approach to coupling strategies for compressible – low Mach number flows. Technical report, Lab. Jacques-Louis Lions, Univ. Paris 6 (France), 2012.
- [14] S. Dellacherie, G. Faccanoni, B. Grec, and Y. Penel. Study of low Mach nuclear core model for two-phase flows with phase transition II: tabulated EOS. In preparation.
- [15] S. Dellacherie, P. Omnes, and P.-A. Raviart. Construction of Godunov type schemes accurate at any Mach number. In preparation.
- [16] S. Dellacherie, P. Omnes, and F. Rieper. The influence of cell geometry on the Godunov scheme applied to the linear wave equation. *Journal of Computational Physics*, 229(14):5315–5338, 2010.
- [17] D. R. Durran. *Numerical methods for fluid dynamics*, volume 32 of *Texts in Applied Mathematics*. Springer, New York, second edition, 2010. With applications to geophysics.
- [18] G. Faccanoni. *Étude d’un modèle fin de changement de phase liquide-vapeur. Contribution à l’étude de la crise d’ébullition*. PhD thesis, École Polytechnique, France, November 2008.
- [19] G. Faccanoni, S. Kokh, and G. Allaire. Modelling and simulation of liquid-vapor phase transition in compressible flows based on thermodynamical equilibrium. *Mathematical Modelling and Numerical Analysis*, 46:1029–1054, September 2012.

- [20] P. Fillion, A. Chanoine, S. Dellacherie, and A. Kumbaro. Flica-ovap: A new platform for core thermal-hydraulic studies. *Nuclear Engineering and Design*, 241(11):4348–4358, 2011.
- [21] W. Greiner, L. Neise, and H. Stöcker. *Thermodynamics and statistical mechanics*. Springer, 1997.
- [22] H. Guillard and C. Viozat. On the behaviour of upwind schemes in the low mach number limit. *Computers & fluids*, 28(1):63–86, 1999.
- [23] O. Le Métayer, J. Massoni, and R. Saurel. Elaborating equations of state of a liquid and its vapor for two-phase flow models. *International Journal of Thermal Sciences*, 43(3):265–276, 2004.
- [24] O. Le Métayer, J. Massoni, and R. Saurel. Modelling evaporation fronts with reactive Riemann solvers. *J. Comput. Phys.*, 205:567–610, 2005.
- [25] E. W. Lemmon, M. O. McLinden, and D. G. Friend. *Thermophysical Properties of Fluid Systems*. National Institute of Standards and Technology, Gaithersburg MD, 20899.
- [26] A. Majda and J. Sethian. The derivation and numerical solution of the equations for zero Mach number combustion. *Combustion science and technology*, 42(3-4):185–205, 1985.
- [27] Y. Penel. Existence of global solutions to the 1d abstract bubble vibration model. Accepted in *Differential and Integral Equations*.
- [28] Y. Penel. *Étude théorique et numérique de la déformation d’une interface séparant deux fluides non-miscibles à bas nombre de Mach*. PhD thesis, Université Paris 13, France, December 2010.
- [29] Y. Penel. An explicit stable numerical scheme for the 1d transport equation. *DCDS-S*, 5(3):641–656, 2012.
- [30] R. Saurel, F. Petitpas, and R. Abgrall. Modelling phase transition in metastable liquids: application to cavitating and flashing flows. *J. Fluid Mech.*, 607:313–350, 2008.